Eidgenössische Technische Hochschule Zürich
Swiss Federal Institute of Technology Zurich

Semester Thesis

Active Magnetic Field Compensation

Author:
Florian Lüthi

Supervisor:
Tobias Thiele

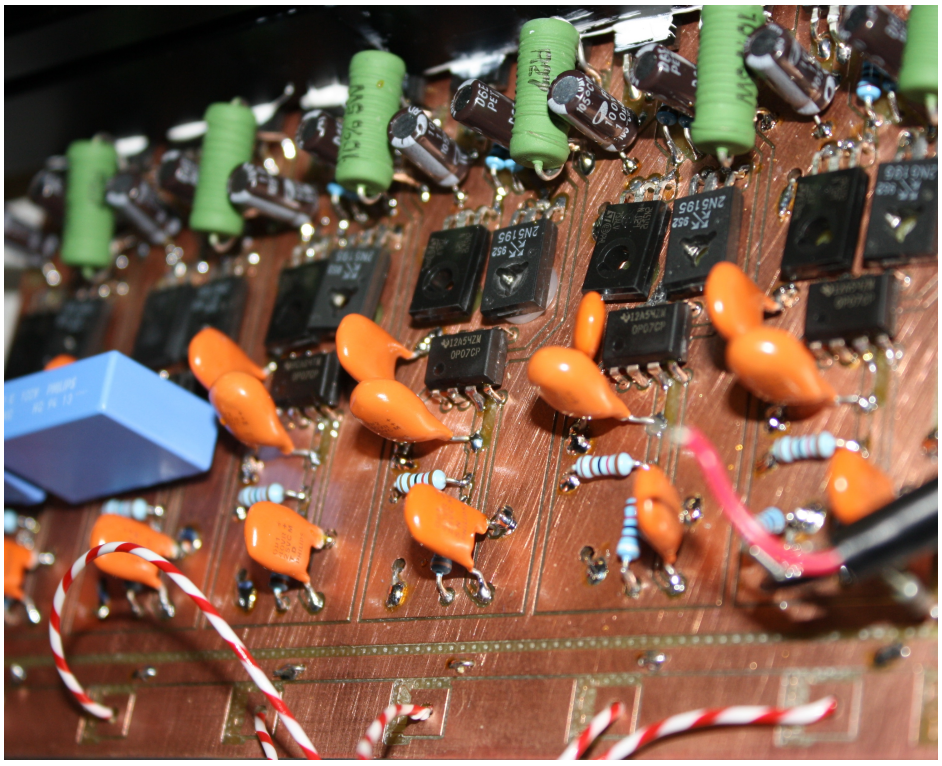

December 2, 2013

Abstract

Magnetic fields have disadvantageous effects on the Rydberg experiment in the Quantum Device Lab trying to couple on-chip microwave photons to Rydberg atoms. In order to minimize these effects, an apparatus for the active compensation of the magnetic field was built during the course of this thesis. It consists of magnetic field sensors that measure the field strength and a feedback procedure that uses the sensor signals to generate a current by means of a voltage controlled current source that flows through a cube of coils producing a magnetic field that counteracts the external magnetic field. At the position of the sensors, the magnetic field can be suppressed to values less than 50 nT.

Contents

1 Introduction

One of many goals of quantum physics today is to build a quantum computer or a quantum simulator in order to simulate quantum mechanical systems as proposed by Feynman in 1982 [1]. There are many different approaches to achieve this goal; for example superconducting circuits using cooper pair boxes [2] or setups using trapped ions as qubits [3]. Also, there are attempts to combine the benefits of different systems in so-called hybrid systems. For example long lifetimes of Rydberg atoms as qubits and fast interactions of the superconducting circuits are tried to be combined in an experiment at the Wallraff group [4]. If this could be realized, the effective lifetime of the superconducting qubits (coherence time of the qubit state compared to the gate time) could be improved. The goal of this semester thesis is to improve the performance of this experiment by building an active magnetic shielding.

1.1 The Experiment

The experiment in [4] generates a pulsed supersonic beam of helium atoms and brings them in a metastable $1s2s^1S_0$ state by an electrical discharge, Figure 1. The beam passes through a skimmer for collimating. A laser pulse of 313 nm excites the metastable He atoms to a np Rydberg state with principal quantum number around $n = 34$. The experimental region including the sample with the microwave waveguide can be cooled to 3 K such that the effect of blackbody radiation is minimized. When the atoms reach a second pair of electrodes a state-selective ionization is done using an electric field pulse. The electrons resulting from this process are then detected in a microchannel-plate detector (MCP). An MCP is basically an electron multiplier with many channels, yielding spatial and temporal resolution of the atomic beam.

Sending microwave pulses through the waveguide while Rydberg atoms are above it induces transitions from the np to the ns state. This again leads to Rabi oscillations between the 33p and 33s states. Figure 2 shows a coherent coupling of the microwave photons in a transmission line and Rydberg atoms, opening the possibilities of implementing quantum gates.

The long term goal of the experiment in [4] is to trap Rydberg atoms above a chip and couple them to superconducting coplanar microwave resonators in order to get very long effective lifetimes. This is not yet possible, but experiments working towards this goal are performed.

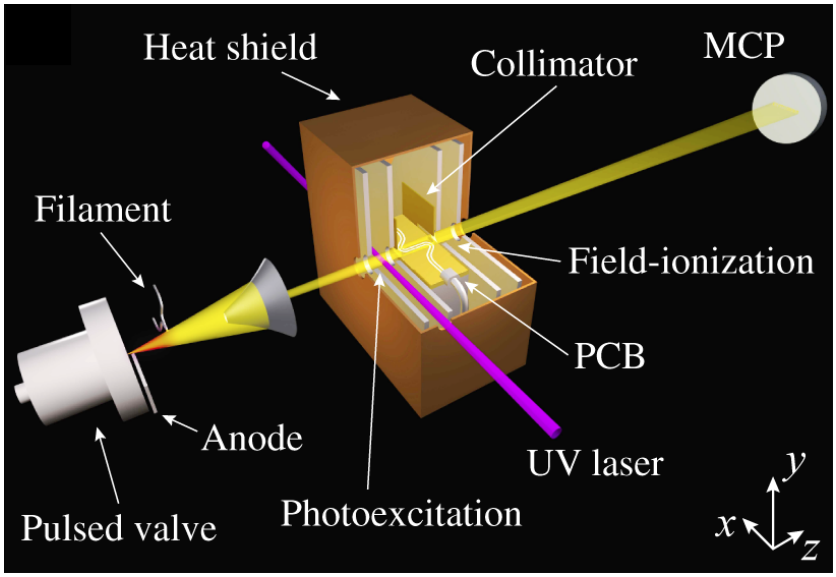

Figure 1: A schematic of the experimental setup used in [4]. A pulsed beam of He atoms is brought to the metastable $1s2s^1S_0$ state, of which some are excited to an $n = 34$ Rydberg state with a 313 nm Laser. They propagate over a PCB with a microwave waveguide and interact with it. The detection is done by a state selective electric field ionization where the resulting electrons are then detected with a MCP. Figure from [4].

1.2 Effects of Magnetic Fields on the Experiment

Several disadvantageous effects may hamper the successful implementation of a Rydberg atom - on-chip microwave interface. One of them is the magnetic field which is present on the one hand due to the magnetic field of the earth and on the other hand from magnets in neighboring laboratories. A brief overview about these effects will be given here. More precise estimations are discussed in Section 2.

Deviation of the Particles The state-selective detection with a high-voltage pulse of 10 ns produces electrons which are detected at the MCP. Between ionization and detection the electrons travel a distance on the order of 20 cm. If there is a nonzero magnetic field perpendicular to the traveling direction of the electrons the Lorentz force will act on them, leading to a deviation of the electrons from the center of the MCP. This can on the one hand lower the detection efficiency as the beam will miss the detector and on the other hand it will disturb the image of the electron beam. Reducing the

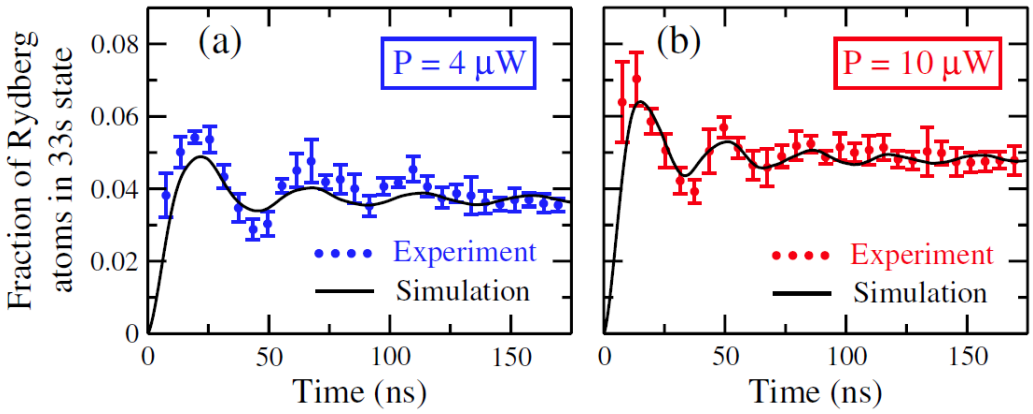

Figure 2: Rabi oscillations between $33s$ and $33p$ state. The fraction of the atoms being in the $33s$ state versus the pulse duration is shown. In (a) the power is $4\,\mu$W, in (b) it is $10\,\mu$W. Black lines are numerical simulations, Figure from [4].

strength of the magnetic field along the path of the electrons will minimize these effects.

Motional Stark Effect As the Rydberg atoms travel in a magnetic field, they experience an effective electric field. This is because of the transformation of the magnetic field from a moving to a stationary frame, $\vec{E}' = \vec{v} \wedge \vec{B}$. The electric field $\vec{E}'$ then causes a Stark shift in the energy levels of the Rydberg atoms. This enery shifts needs to be taken into account when trying to drive Rabi oscillations between high lying Rydberg states.

2 The Problem

In this section we will first estimate the impact of two effects due to the magnetic field on the experiment. As mentioned before, these effects are the deviation of the electrons due to the Lorentz force and the motional Stark effect. Also, the approximations done in the estimations will be analyzed and the results of these estimations will be discussed.

2.1 The Magnetic Field in the Lab

The building in which the experiment is set up contains many laboratories, and some of them close by have setups with very strong magnets with mag-

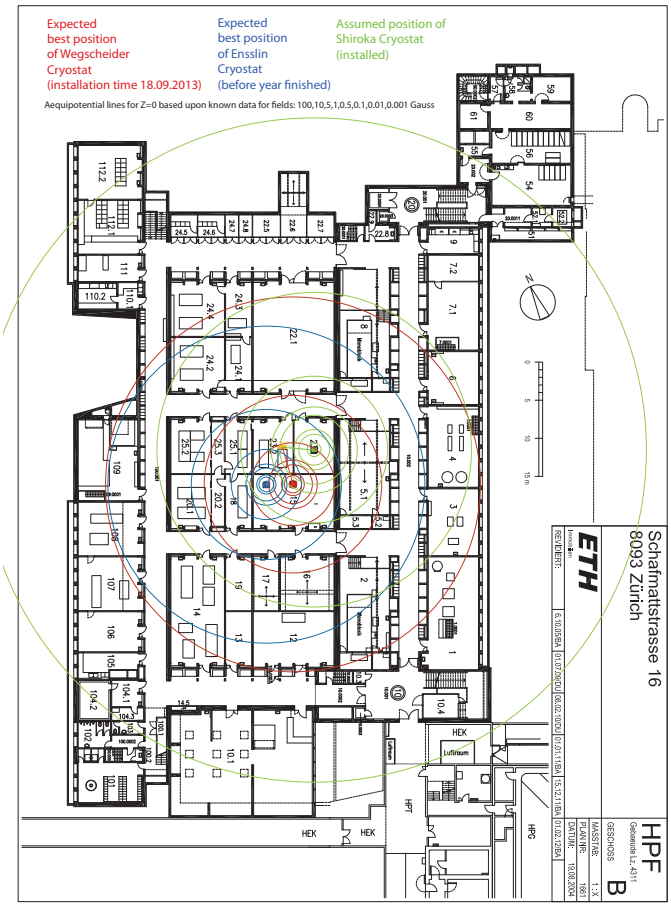

Figure 3: Positions of the magnets of the other groups and estimated field strengths. The position of the experiment is marked with an orange spot.

netic field magnitudes of up to 12 T. Finite stray magnetic fields of these machines will have negative effects on the experiment. The positions of the closest magnets and an estimation of their field strengths are indicated in Figure 3. All in all, the magnitude of the field of each magnet is expected to be on the order of the magnetic field of the earth, $\approx 35\,\mu\mathrm{T} = 0.35\,\mathrm{G}$.

We measured the field strengths in our laboratory at several positions, Figure 4, and created a schematic map with indicated field strengths in the laboratory. The vectors show the direction and amplitude of the field in the plane parallel to the floor, 90 centimeters above ground. The color of the plot indicates the field strength in z-direction. The strong field in the lower left corner indicates that the nearby magnet of Shiroka is running. The magnetic

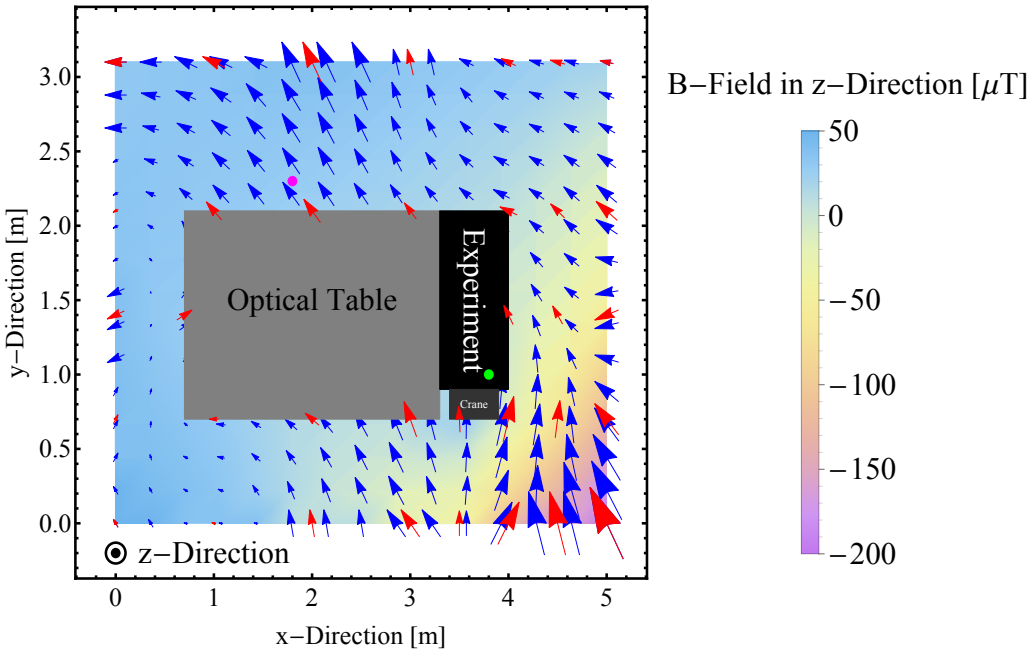

Figure 4: The magnetic field in the Laboratory. The vectors indicate the field strength in the x-y-plane. Red vectors are points measured at a height of 0.9 m, blue vectors are interpolated. The background color indicates the field strength in z-direction. The black box indicates the experiment, the light gray box is the optical table and the dark gray is a crane supporting the experiment. The magenta and green circles indicate the positions of the measurements in Figures 5 and 6.

field of it is damped due to the fact that many metallic parts - including a big crane - in the vicinity of the experiment were magnetized.

This magnet had to be removed from the lab due to security issues, since the field outside the lab was stronger than 5 G, and was therefore posing a danger to persons using a cardiac pacemaker [5]. Although the magnet is now removed, it caused permanent magnetization of many things in the laboratory. For example many anchor rails ("Jordalschienen") on the wall have maximal B-Fields of up to 40 G, the table legs 20 G and the crane produces a magnetic field of up to 10 G. The optical table has a magnetic moment that yields a B-Field of around one Gauss close to the table. This is disadvantageous, as the demagnetization of such big objects is really difficult and expensive. Also, many screws on top of the vacuum system are magnetized. The hull of the vacuum system is not magnetized, because it is made of stainless steel.

The magnet of the Wegscheider-Group (a Bruker Ascend, 12 T) is positioned at around (-1, 1) m with respect to the coordinate system in Figure 4. In Figure 5 the change of the magnetic field at position $(1.8, 2.3, 0.3)$ m (magenta circle in Figure 4) is shown when the magnet of the Wegscheider-Group is ramped from 0 to 12 T with 0.3 T/min. We observe a change in the field strength of about 20 μT in all directions, and therefore a change of the absolute field strength $\Delta B = \sqrt{\Delta B_x^2 + \Delta B_y^2 + \Delta B_z^2} \approx 37\,\mu$T. The position of the sensors is about 3 meters closer to the magnet as the actual experiment, therefore the change of the Field in Figure 5 is a bit stronger than expected at the position of the experiment.

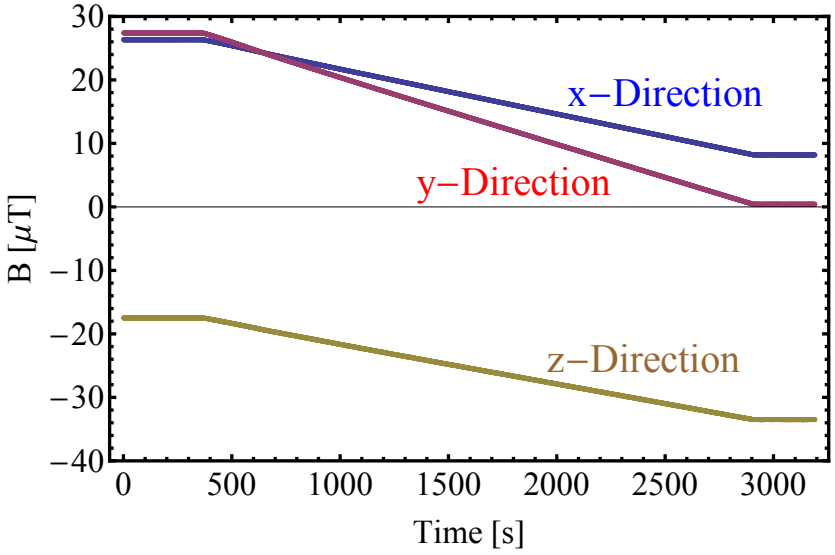

Figure 5: Change of the magnetic field over time when the Magnet of the Wegscheider Group is ramping up. The coordinate system is the same as in Figure 4. The position of the sensor is approximately $(1.8, 2.3, 0.3)$ m (magenta circle in Figure 4), also with respect to the coordinate system in Figure 4.

Figure 6 shows the field strength at the position of the experiment, approximately $(3.8, 1.0, 1.4)$ m (green circle in Figure 4), while the magnet is being ramped down from 12 to 0 T. The initial and final field strengths are different from Figure 5 because the position has changed and also it is likely that there are several magnetized pieces around the experiment. The magnetic field in y-direction stays approximately constant because this direction is orthogonal to the field produced by the magnet. The total change in the magnetic field is in this case $\approx 18\mu$ T. Thus, it is approximately twice as big

as expected in Figure 3, due to the fact that the magnet is positioned closer than indicated. This corresponds to an additional magnetic field with about half the strength of the field when the magnet is turned off ($\approx 39\mu\,\mathrm{T}$).

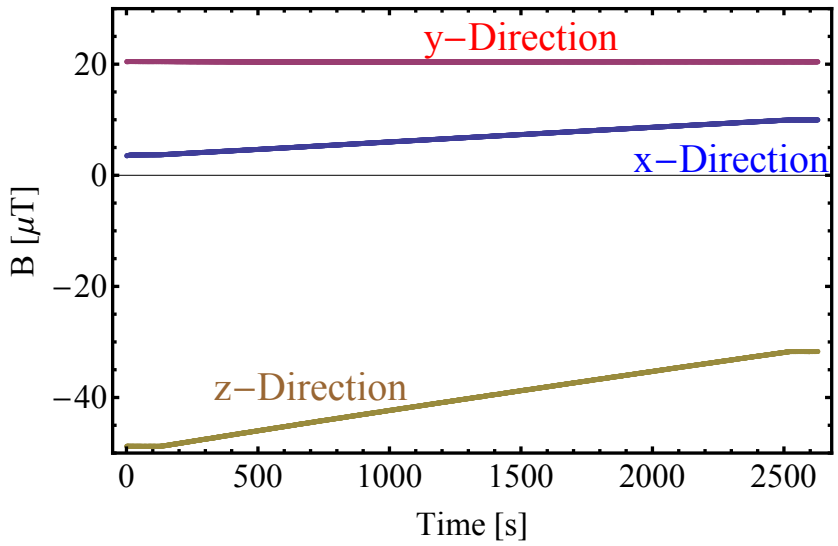

Figure 6: Change of the magnetic field over time at the experiment when the Magnet of the Wegscheider Group is ramping down. The position of the sensor with respect to the coordinate system in Figure 4 is approximately given as $(3.8, 1.0, 1.4)\,\mathrm{m}$ (green circle in Figure 4).

2.2 Estimation of the Deviation of the Electron Beam

In the experiment, the detection of Rydberg atoms involves electrons flying over a distance of 20 cm. We will now briefly estimate the deviation of this beam under the influence of a B-field. If the deviation of the beam is too big, some of the particles will miss the circular MCP with radius 2 cm and thus lower the signal. This is especially relevant when pictures of the Rydberg atomic beam are made, since then an ion lens will defocus the electron beam. In the following we will link the deviation of the electrons to the strength of the B-Field, enabling us to define an upper limit for the field strength such that only little loss is introduced by this effect.

To do this, we fist assume that the electrons move in x-direction and the magnetic field points in z-direction - which yields a maximal deviation. The equation of motion is therefore given by the Lorentz Force,

$$\vec{F} = m \cdot \ddot{\vec{x}} = -e \cdot \vec{v}_0 \wedge \vec{B}$$

where $\vec{F}$ is the force, m is the electron mass, $\ddot{\vec{x}}$ is the acceleration of the electron, e is the electron charge, $\vec{v_0} = v_0 \cdot \hat{e}_y$ the velocity of the electrons in y-direction and $\vec{B} = B \cdot \hat{e}_z$ is the magnetic field in z-direction. If we perform the vector product and have a look at the y component, we get that

$$m \cdot \ddot{x}_x = -e \cdot v_0 B.$$

Assuming that the deviation is small compared to the distance the electrons travel we can make the approximation that the speed of the electrons at time t in x-direction, $\dot{x}_x(t)$, is the acceleration of the electrons integrated with respect to time,

$$\dot{x}_x(t) = \int_0^t \ddot{x}_x(t')\mathrm{d}t' = \int_0^t \frac{-e}{m} \cdot v_0 B \mathrm{d}t' = \frac{-e}{m} \cdot v_0 B \cdot t.$$

If we would not make this approximation, we would have to account for the fact that the electrons will experience a reduced acceleration in x-direction and get some acceleration in y-direction instead for $t > 0$. This is because the velocity of the electrons stays constant, but they would move in a circle under the influence of a magnetic field. Nonetheless, for small deviations of the electrons in x-direction over the whole traveling distance this simple model suffices.

In a next step we integrate the velocity of the electrons, $\dot{x}_x(t)$, to get the deviation with respect to the y-axis at time t,

$$x_x(t) = \int_0^t \dot{x}_x(t')\mathrm{d}t' = \frac{-e}{m} \cdot v_0 B \cdot \frac{t^2}{2}. \tag{1}$$

The distance l the electrons travel along the y-axis is $\approx$20 cm. Inserting the voltage $U = 1200\,\mathrm{V}$ with which the electrons are accelerated, one can then calculate the time needed to travel over this distance. Equating the potential energy with the kinetic energy at full speed v_0 yields

$$eU = \frac{1}{2} m_e v_0^2,$$

resulting in a velocity

$$v_0 = \sqrt{\frac{2eU}{m_e}} = \sqrt{\frac{2 \cdot 1.6 \cdot 10^{-19}\,\mathrm{C} \cdot 1200\,\mathrm{V}}{9.1 \cdot 10^{-31}\,\mathrm{kg}}} = 2.1 \cdot 10^7\,\frac{\mathrm{m}}{\mathrm{s}}.$$

Because v_0 is an order of magnitude smaller than the speed of light we justify our non-relativistic approach to determine the velocity. The time T the electrons require to travel the distance l is then given by $T = l/v \approx 10\,\mathrm{ns}$.

Finally we are interested in the deviation at distance l, which is approximately given as $x_x(T)$. We can insert numbers in Equation (1) to get an idea of the deviation at different field strengths.

- 1 G=100 μT (worst case scenario when all magnets are on) yields a deviation of 1.85 cm.
- 0.35 G=35 μT (the earth magnetic field) yields a deviation of 6.5 mm.
- 0.01 G=1 μT (what should be easily realizable if the apparatus is well calibrated) yields a deviation of 0.2 mm.

We can see that the approximation should do fine because the deviation is an order of magnitude smaller than the traveling distance. Therefore the difference between the approximated parabolic trajectory and the true circular movement of the electrons is negligible.

In conclusion we see that it indeed can lead to a problem when big magnetic fields are present as the beam deviation is comparable to the size of the MCP screen. If the deviation is getting too big it can lead to the electrons missing the MCP screen, thus rendering us unable to detect them.

2.3 Estimation of the Motional Stark Effect

The Stark effect is the shift in energy for atoms in an electric field. Here we are considering the effects of a magnetic field on moving Rydberg atoms, and thus a brief discussion on the Galilean transformation is given. Then, using this transformation, we will estimate the effect of a magnetic field perpendicular to the propagation direction of the atoms.

The Galilean transformation is the (classical) transformation between two frames of reference which are only different due to a constant motion of one system to the other. This approximation is justified because the atoms move with 1750 m/s, well below the speed of light. Let's call the laboratory frame F, where we have a static magnetic field $\vec{B}$, and call the frame of the particles F', traveling with a velocity $\vec{v}$. Then, the electric field $\vec{E'}$ in the particle frame is (given by the Galilean transformation, compare [6])

$$\vec{E'} = \vec{E} + \vec{v} \wedge \vec{B}.$$

To obtain an energy shift, we need to estimate the dipole moment of a Rydberg state. In the experiment, there are only Rydberg state with small angular momentum l. Therefore we can estimate the dipole moment $\vec{d}$ of the atoms (compare [7]) to be

$$\vec{d} = \frac{3}{2} n(n-1) \cdot a_0 e \cdot \hat{e},$$

where n is the principal quantum number of the Rydberg states, e the electron charge, a_0 is the Bohr radius and $\hat{e}$ is a unit vector pointing in the direction of the dipole.

The energy shift U_{dip} is then given by

$$U_{dip} = \vec{d} \cdot \vec{E}'.$$

Now we assume that the magnetic field is just the earth magnetic field, and that it is pointing perpendicular to the propagation direction of the atoms. Further on we assume that there is no electric field in the laboratory frame, $\vec{E} = \vec{0}$ and that the dipole moment is parallel to the electric field $\vec{E}'$. Using $n = 33$ and the velocity $v = 1750\,\mathrm{m/s}$ of the Rydberg atoms we get

$$\begin{aligned} U_{dip} &= \frac{3}{2} n(n-1) \cdot a_0 e \cdot \hat{e} \cdot \vec{v} \wedge \vec{B} \\ &= \frac{3}{2} n(n-1) \cdot a_0 e \cdot vB = 8.2 \cdot 10^{-28}\mathrm{J}, \end{aligned}$$

which corresponds to a frequency shift $U_{dip}/h \approx 1.2\,\mathrm{MHz}$. This estimation gives an upper bound, since the calculation takes only a linear stark shift into account. The low-l states in Helium reveal a quadratic stark effect due to a non-zero quantum defect which is less sensitive to electric fields weaker than $1\,\mathrm{V/cm}$. The effective contribution of the moving stark effect will be a shift on the order of $\sim 100\,\mathrm{kHz}$.

3 The Concept

This section will discuss different possibilities of magnetic shielding and an evaluation on suitability for our choice of active magnetic shielding with Helmholtz coils. Also we present a theoretical model for the magnetic field within the area that needs to be compensated.

3.1 Passive Shielding

As we are facing only static or very slowly varying magnetic fields it is not enough to just have a layer of metal around the target area which should be protected (Faraday cage), because the magnetic field will penetrate the metal and render this kind of protection ineffective. Only fields with a finite frequency are damped well with a metal layer of thickness greater than the corresponding skin depth of the material due to eddy currents at the surface of the metal. The skin depth δ is given as

$$\delta = \sqrt{\frac{2\rho}{2\pi f \mu}}$$

where ρ is the resistivity, $\mu = \mu_r \cdot \mu_0$ is the magnetic permeability of the conductor and f is the frequency of the field. Inserting the values for stainless steel 316 [8], [9] (that is the material of which the hull of the experiment is made of) yields

$$\delta = \sqrt{\frac{2 \cdot 7.5 \cdot 10^{-7}}{2\pi \cdot 10^5 \cdot 1.4 \cdot 4\pi \cdot 10^{-7}}} = 1.2\,\text{mm}$$

for a frequency of $f = 100\,\text{kHz}$. Therefore we can conclude, as the hull has a thickness of 3 mm, that high frequency fields are damped well.

In order to get a good damping for slowly varying and constant (dc) fields metals with a high magnetic permeability are necessary. It can be shown [10] that the magnetic field inside a spherical shell is damped with respect to the external field as

$$\vec{H}_{in} = \eta \vec{H}_0 \quad \text{where} \quad \eta = \frac{9}{2} \frac{1}{\left(1 - \frac{a^3}{b^3}\right) \mu}$$

in the limit of high magnetic permeability, $\mu \gg 1$, where a and b are the inner respectively outer radii of the shielding sphere. As η scales with μ^{-1} a reasonable damping can be achieved if a shielding material with high magnetic permeability, for example Mu-metal with $\mu_r \approx 80'000$-$100'000$ (compare with several thousand for steel or a few for stainless steel [11]) is chosen.

A major problem arises as we introduce holes into the sphere, which is necessary to access the experiment by laser beams. The figure of merit here is the unshielded solid angle, leaving the only possibility to counteract the effect of these holes in making chimneys around the holes. This is disadvantageous, since the chimneys need to have about five times the length of the diameter of the hole to compensate the effect of the hole well [11]. From a designing point of view this gets difficult to realize and becomes unhandy, especially as some holes need to be rather big (diameter of more than 5 cm). The corresponding chimneys need then to be rather long, which will again be difficult to place around the experiment.

Due to these reasons the decision was made against passive shielding.

3.2 Active Compensation

Another possibility of compensating stray magnetic fields is to apply a magnetic field created by an artificial source, e.g. a coil configuration of the same strength but opposite direction that counteracts the source due to the superposition principle. The shielded area only has a small remaining magnetic field.

The basic idea here is to implement a feedback procedure that measures the field in the target area. The data is sent to a central unit which in turn feeds a signal back to the artificial source. If the feedback is well done it can then control the magnetic field such that it gets very small in the designed region.

The difference between high and low frequency magnetic fields has to be made again. Dc and very slowly varying fields can be suppressed with active compensation easily just by applying a current through the artificial source. But this gets challenging for higher frequencies because of two reasons. The first and most important one is that current sources can not provide a large current immediately upon request, but usually need a finite time to supply the current. The second reason why one can not compensate high frequency fields actively is that the usually artificial sources have high inductance. A high inductance leads to stronger magnetic fields at a given current, but the change in the magnetic field will be slower. Therefore we have a trade-off: A low inductance requires a high current, which requires a finite amount of time to ramp up, and a high inductance prevents the field from building up quickly.

High frequency fields will be damped reasonably well due to the metallic hull of the vacuum system of the experiment acting as a Faraday cage. Since the experiment is phase locked onto the line of the power supply, the 50 Hz noise is expected to be of negligible effect.

Because slowly varying magnetic fields can be compensated well actively using a coil arrangement we decided to build an active compensation. Another advantage of this method is that it does not depend very much on the exact geometry of the experiment, because the coils can be placed around the experiment.

3.3 Magnetic Field of Rectangular Helmholtz Coils

In order to create a homogeneous B-Field in the target area six rectangular coils in a Helmholtz-like configuration, arranged in a cubic geometry are used, Figure 7a. This configuration will enable us to to control the B-Field in all directions. As the coils are rectangular and the distance between them is fixed, the optimal Helmholtz configuration is not satisfied [12]. In the following, an estimation of the field created by these coils is presented and compared to the measured values of the field strength for a fixed current through the coils.

Derivation of the B-Field of the Coils In this section the analytical expression for the strength of the magnetic field will be derived. First, we

have a look at the magnetic field that a flat, rectangular coil produces on its axis. Later on, we will look at the field that arises when two such coils are placed in a Helmholtz-like configuration, again restricted to the common axis of the coils. We consider two coils at a distance of $\pm a \cdot \hat{e}_x$ from the origin. Each coil extends in y-direction by $2 \cdot b$ and in z-direction by $2 \cdot c$, Figure 7b.

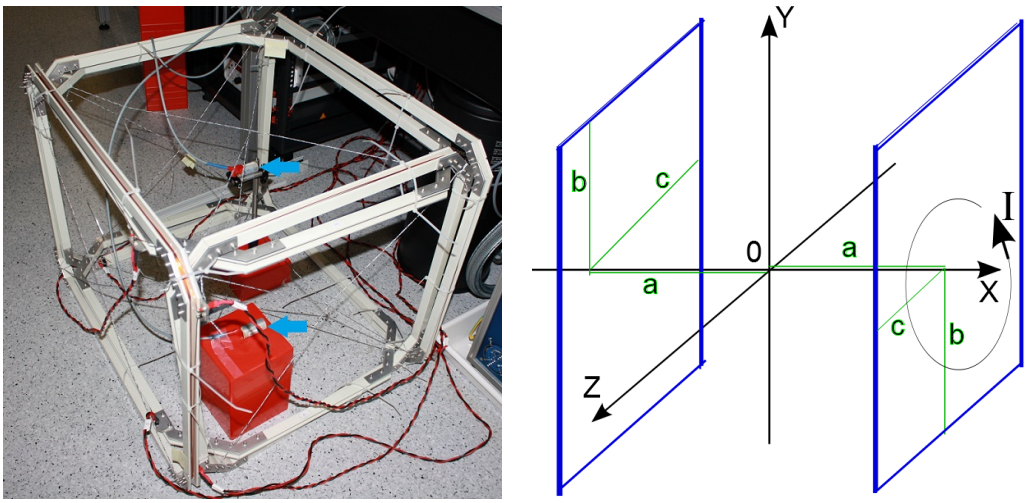

(a) The six coils used in a rectangular Helmholtz configuration form a cube. The arrows indicate the magnetic field sensors.

(b) This figure shows the geometry used. Note that the total side lengths are $2a$, $2b$ and $2c$, respectively.

Figure 7: The real cube of Helmholtz coils and the geometrical model used.

To calculate the field on the axis created by one coil we start from the Biot-Savart law,

$$\vec{B}(\vec{r}) = \frac{\mu_0}{4\pi} \int_V \frac{\vec{J}(\vec{r'}) \wedge (\vec{r} - \vec{r'})}{|\vec{r} - \vec{r'}|} \mathrm{d}\vec{r'} \tag{2}$$

where $\vec{J}(\vec{r})$ is the current density at point $\vec{r}$ and the integration volume V is the whole $\mathbb{R}^3$. As we are only interested in the x-component of the magnetic field along the x-axis, $B_x(x)$, we can set

$$\vec{r} = \begin{pmatrix} x \\ 0 \\ 0 \end{pmatrix}.$$

As currents flow only along the edges of the coil, the integration in Equation (2) is reduced to a path-integration along the coil-edge. Thus, the current density is

$$\vec{J}(\vec{r'})\mathrm{d}\vec{r'} = N \cdot I \cdot \mathrm{d}\vec{l},$$

where I is the current that flows through the coils and N is the number of windings of the coil and $\mathrm{d}\vec{l}$ denotes the path-element of the integration. The

vector product in Equation (2) therefore yields

$$\left[\vec{J}(\vec{r})) \wedge (\vec{r}-\vec{r'})\mathrm{d}\vec{r'}\right]_x = NI\left[\begin{pmatrix}\mathrm{d}x'\\ \mathrm{d}y'\\ \mathrm{d}z'\end{pmatrix} \wedge \begin{pmatrix}x-x'\\ -y'\\ -z'\end{pmatrix}\right]_x = NI\cdot(-z'\mathrm{d}y' + y'\mathrm{d}z').$$

Substitution into Equation (2) gives us

$$B_x(x) = \frac{\mu_0 NI}{4\pi}\oint_\gamma \frac{\left(\mathrm{d}\vec{l}\wedge(\vec{r}-\vec{r'})\right)_x}{|\vec{r}-\vec{r'}|^3} = \frac{\mu_0 NI}{4\pi}\oint_\gamma \frac{-z'\mathrm{d}y' + y'\mathrm{d}z'}{\left((x-x')^2+y'^2+z'^2\right)^{3/2}} \tag{3}$$

where γ is the path of the current, respectively the edges of the coils. We will perform the integral for the coil at $+a\cdot\hat{e}$. We insert the geometry parameters and split the integral into four parts, one for each side. Two parts are for the current traveling along the y- and $-y$-direction, the others are for the current traveling along the z- and $-z$-direction. The current is chosen to travel clockwise when looking in $+x$-direction. As the path is orthogonal to either y or z, one of the $\mathrm{d}y$ or the $\mathrm{d}z$ will yield no contribution to the integral. Two of the three initial integration variables have fixed values that can be inserted into Equation (3). To clarify things, we for example look at the part of the path with positive x and y values. There, we integrate z' from $-c$ to c, and we insert $x'=a$ and $y'=b$ (compare Figure 7b). Doing this analogously for the other parts of the path gives an x-component of the magnetic field along the x-axis for one coil at position $x=a$ as

$$\begin{aligned}
B_{x,1}(x,a) &= \frac{\mu_0 NI}{4\pi}\oint_\gamma \frac{-z'\mathrm{d}y' + y'\mathrm{d}z'}{\left((x-x')^2+y'^2+z'^2\right)^{3/2}} \\
&= \frac{\mu_0 NI}{4\pi}\left[\int_{-c}^{c}\frac{b\cdot\mathrm{d}z'}{((x-a)^2+b^2+z'^2)^{3/2}} + \int_{b}^{-b}\frac{(-c)\cdot\mathrm{d}y'}{((x-a)^2+y'^2+c^2)^{3/2}}\right. \\
&\quad \left. + \int_{c}^{-c}\frac{(-b)\cdot\mathrm{d}z'}{((x-a)^2+b^2+z'^2)^{3/2}} + \int_{-b}^{b}\frac{-(-c)\cdot\mathrm{d}y'}{((x-a)^2+y'^2+c^2)^{3/2}}\right],
\end{aligned}$$

which can be simplified to

$$B_{x,1}(x,a) = \frac{\mu_0 NI}{2\pi}\left[\int_{-c}^{c}\frac{b\cdot\mathrm{d}z'}{((x-a)^2+b^2+z'^2)^{3/2}} + \int_{-b}^{b}\frac{c\cdot\mathrm{d}y'}{((x-a)^2+y'^2+c^2)^{3/2}}\right].$$

These are standard integrals which can be solved analytically. The solution is

$$B_{x,1}(x,a) = \frac{\mu_0 NI}{2\pi}\frac{2bc}{\sqrt{(x-a)^2+b^2+c^2}}\left[\frac{1}{((x-a)^2+b^2)} + \frac{1}{((x-a)^2+c^2)}\right]. \tag{4}$$

In order to get the x-component on the x-axis for the field of two coils, we add the fields of one located at $x = -a$ and the other one located at $x = a$. Due to the superposition principle we get

$$\begin{aligned} B_x(x) &= B_{x,1}(x,a) + B_{x,1}(x,-a) \\ &= \frac{2bc\mu_0 NI}{2\pi}\Big[\frac{1}{\sqrt{(x-a)^2+b^2+c^2}}\Big(\frac{1}{((x-a)^2+b^2)} + \frac{1}{((x-a)^2+c^2)}\Big) \\ &\quad + \frac{1}{\sqrt{(x+a)^2+b^2+c^2}}\Big(\frac{1}{((x+a)^2+b^2)} + \frac{1}{((x+a)^2+c^2)}\Big)\Big]. \end{aligned}$$

A more general way of this formula can be obtained assuming that the currents and windings of the two coils are different. To get the formula for the B-Field of two coils with the same geometry parameters (compare Figure 7b) but different currents and numbers of windings we start again with Equation (4). Considering the current I and number of windings N not to be fixed, but being parameters, $B_{x,1}(x,a)$ becomes $B_{x,1}(x,a,I,N)$. Using the superposition principle again, we obtain

$$\begin{aligned} B_x(x) &= B_{x,1}(x,a,I_1,N_1) + B_{x,1}(x,-a,I_2,N_2) \\ &= \frac{2bc\mu_0}{2\pi}\Big[\frac{I_1N_1}{\sqrt{(x-a)^2+b^2+c^2}}\Big(\frac{1}{((x-a)^2+b^2)} + \frac{1}{((x-a)^2+c^2)}\Big) \\ &\quad + \frac{I_2N_2}{\sqrt{(x+a)^2+b^2+c^2}}\Big(\frac{1}{((x+a)^2+b^2)} + \frac{1}{((x+a)^2+c^2)}\Big)\Big]. \end{aligned} \tag{5}$$

To test how well Equation 5 predicts the magnetic field in the cube, the magnetic field along the coil axis was measured every five centimeters with a fixed current of 1.5 A flowing through the coils. Then, the value of the magnetic field with no current applied was subtracted from the data at each point to get the magnetic field that is produced only by the coils. This procedure was done for each spatial direction.

In Figure 8 the solid lines correspond to the theoretical curves given in Equation (5) and the dots correspond to measured values along the respective axis. The errors in y-direction are larger because the sensor could not be fixed. The largest error source for the field is a possible misalignment of both the coils and the sensor with respect to the coil axis.

The parameters used are $I = 1.5\,\mathrm{A}$, $a = 32.5$, $b = 25$ and $c = 27.5\,\mathrm{cm}$. The winding numbers are $N_1 = 31$ for the coil at $+a$ and $N_2 = 30$ for the one at $-a$ in x-direction. For the coils in y-direction $N_1 = 30$ for the one at $+b$ and $N_2 = 32$ for the one at $-b$. Both coils in z-direction have 10 windings.

All in all the theoretical curve fit good to the measurement values and are within the error boundaries, showing that the magnetic field created by the coils is well understood.

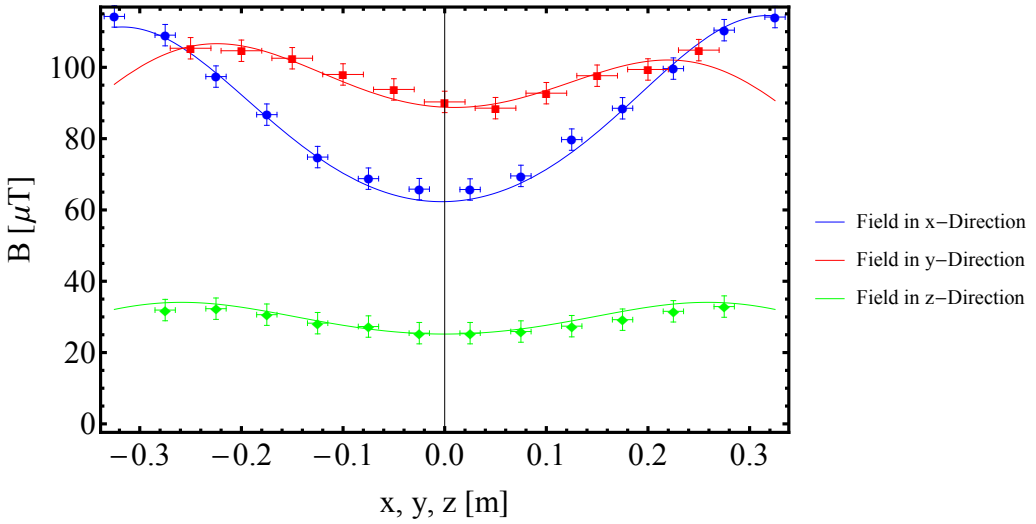

Figure 8: The effective magnetic field in the Helmholtz Coils in the three spatial directions. Measured values are represented with dots, the theoretical value from Equation 5 are the solid lines. The field in x-direction is measured while varying the position on the x-axis of the Helmholtz pair, y- and z-fields analogously.

As a side note it is to mention that first the values of the measured magnetic field in y-direction did not behave as expected. It turned out that the field was distorted by the metallic (but non-magnetic) mount of the sensor.

3.4 Possible Ways of Compensation

Detecting the Magnetic Field There are two different possible methods to measure a magnetic field. The first method is to use one sensor and place it in the middle of the target area of the Helmholtz field. This gives the value of the field strength in the center of the area that one wishes to compensate.

The second method is to use a differential measurement. For this, two sensors are required, and they need to be placed at the border of the area that one tries to compensate. Now one can use the additional information to compensate the field inside the area better, especially if field gradients are present.

Driving the Coils Using a differential measurement, there are two different possibilities to operate a pair of Helmholtz coils. One can either wire them up in series, or one can control each coil separately. The advantage of driving the coils in series is that less current sources are required, since each direction needs only one current source. But on the other hand side one can again just compensate a constant magnetic field, and the strengths of a differential measurement would be neglected.

However, if one chooses to control all the coils separately it is possible to compensate every magnetic field with a constant gradient within the target area.

The difference between these two types of driving the coils is shown in Figures 9 and 10, where the geometry parameters from Section 3.3 are used to model. In both Figures the green curve shows a Helmholtz field where both coils have the same current. In Figure 9, this field is used to compensate a constant magnetic field (magenta). The red curve is obtained by subtracting the magenta field from the green line and shows the resulting field, which is very small and has a vanishing first derivative at $x = 0$. The blue curve, obtained by subtracting a gradient field from the Helmholtz field, shows the resulting field if a gradient field (cyan) is applied with the same current flowing through the coils. It has a nonzero first derivative around zero, although the field amplitude is still zero there.

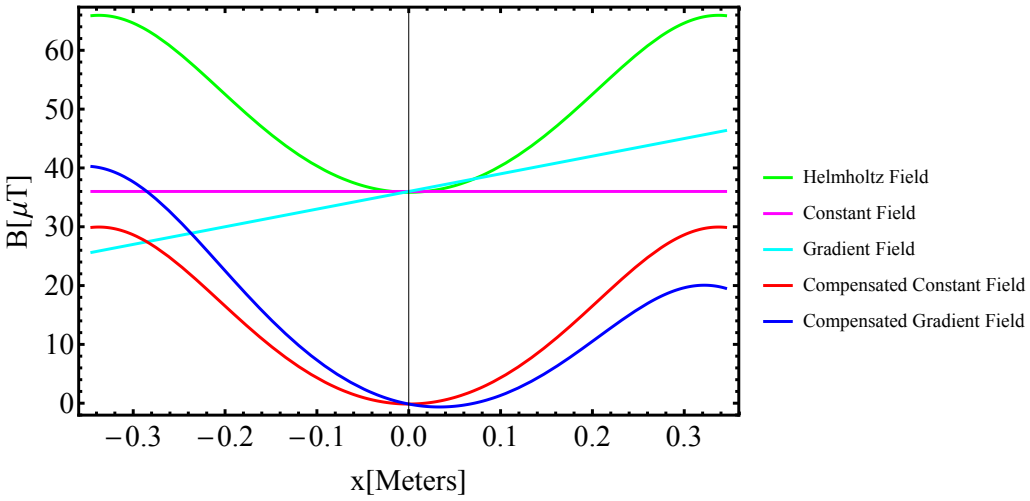

Figure 9: Simulation of the field of a rectangular Helmholtz coil when both coils are driven with the same current. The red and blue curves show the effective field when the Helmholtz pair is used to compensate a constant field respectively a field with constant gradient.

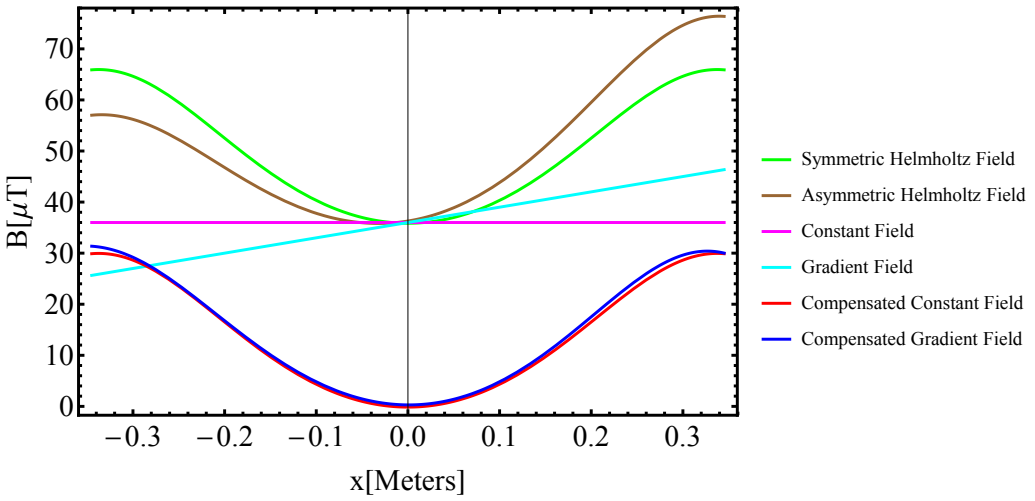

Figure 10: Simulation of the field of a rectangular Helmholtz coil when the coils are driven with different currents (brown line). The red and blue curves show the effective field when the Helmholtz pair is used to compensate a constant field respectively a field with constant gradient.

In Figure 10, the green, cyan, magenta and red curves are still the same as in Figure 9 (explained above), but the brown curve shows now the field resulting from two different currents flowing through the two coils. The blue curve then shows the resulting field, which now also has a vanishing first derivative and amplitude at $x = 0$.

Thus, we can conclude that it is the better choice to use a differential measurement and a differential compensation in order to get rid of the magnetic field as good as possible. Up to first order, spatially varying magnetic fields can be compensated with a differential setup, whereas a normal setup can only compensate a constant magnetic field.

4 The Feedback

Active compensation requires more elaborate setups than passive shielding because a feedback is required, Figure 11. Sensors measure the magnetic field, their analog signal is read out and digitalized by an input card. The digitalized input signal is then processed and a control signal determined. It is sent to an analog output card that in turn creates an analog signal. This signal is used to control a voltage controlled current source (VCCS) which supplies the current that will create a magnetic field in the coil cube. This feedback process will be discussed step by step in this section.

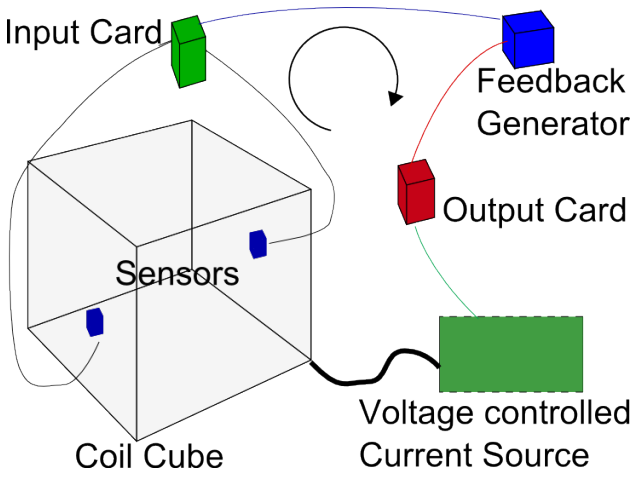

Figure 11: A schematic drawing of how the feedback is realized. The sensor signal is processed, and an output signal then controls a current source and therefore regulates the current flowing through the coils. This current produces a magnetic field, and the feedback is complete.

4.1 The Sensors

Normal hall bar sensors (not including two dimensional electron gas Hall sensors) are too insensitive for this application, as we are interested in fields smaller than one μT. Therefore two tri-axial flux-gate sensors FLC3-200 of Stefan Mayer Instruments are used [13]. These sensors have a measurement range of $\pm 200\,\mu$T, and need to be powered with a 6 mA current at 12 V. Their output voltage scales with 1 V per 35 μT with respect to half the supply voltage. The accuracy is $\pm 0.5\,\mu$T.

4.2 The Input Card

A National Instruments analog input card, a NI 9205, with 32 input channels that accepts voltages up to ± 10 V was used [14]. It works as an analog to digital converter with a 16 Bit input. In principal, one could use a measurement of the voltages with respect to the ground of the card. But the sensors give their signal with respect to a +6 V reference with respect to ground of the voltage source. Therefore a differential measurement is required for all directions.

4.3 Software

In order to process the signals that the input card digitizes a piece of software is needed. Here we use Lab View by National Instruments [15]. Lab View is a visual based programming environment useful for labor-related applications.

The Tasks Used For communication with the NI cards (input and output cards) Lab View uses tasks. In these tasks the physical channels of the in- and output ports are specified and at which rate the samples should be read out and written.

In our case we want to read samples from six channels, corresponding to the two times three sensor outputs. Also, we do not need arbitrarily fast sampling rates, as the voltage controlled current source (VCCS) has a response time of $\approx 25\,\text{msec}$, which we get from the pulse response measurement described in Section4.5, Figure 21. Therefore once every second 100 samples per channel are read out and averaged. They are then processed further to create the output signal.

The writing channel is set to a writing rate of one second. A faster rate would not make sense as the VCCS can not operate at higher speeds.

The Feedback Control Dependent on the input signal, an according response needs to be made in order to reduce the magnetic field in the cube. The feedback used here is an Integrator (I-control), that just tries to pull the magnetic field that a sensor measures to a given set-point. It does that for each direction separately, meaning that the X signal of sensor 1 will just influence the output voltage determining the current through the coil facing in x-direction which is closest to it. The I-control works in a way that it adds half of the actual error signal voltage, obtained from the sensors, to the output voltage. The output voltage is then stored, and in the next iteration of the program - one second later - again half the error signal is added to the output voltage. Like this, one gets principally arbitrarily close to the desired value of the magnetic field. In order to get a stable solution and prevent oscillations around a value or a "beating" between two coils (due to crosstalk arising from misalignment and non-uniform fields of the coils) a threshold is introduced. If the error signal is below this threshold it will not result in a change of the output voltage.

In order to get a near-zero magnetic field in the middle of the cube, and not just at the sensor positions, the set-point (offset of the magnetic field) can be chosen arbitrarily. It is handled in a way that the sensor signal from the input is altered such that the error signal is zero when the sensors are on

the desired level of the magnetic field. This is easier than altering the output voltage, because then the feedback would again try to compensate the offset.

The User Interface Lab View directly creates a more user friendly view allowing the handling of the running program, Figure 12. In the user interface for the magnetic field control program, there are two big wave charts. The first one indicates the magnetic field the sensors are currently measuring and the lower one displays the output voltages. Further on, there is an indicator that estimates how much current is flowing at the moment through the VCCS, separated for positive and negative polarization. The iteration counter shows how many iterations (here one iteration takes one second) the program has already performed since it was started. On the lower end of the front panel error messages are displayed (not visible in Figure 12).

There are several things that the user can control. The first is the location of the text file where the sensor and voltage output data should be stored. Then the update period can be altered, this is the time duration in milliseconds the program waits until it performs another iteration. The suggested value is 1000 ms, meaning that every second the magnetic field is measured and an adequate feedback is provided. The offset of the magnetic field can be chosen on the right hand side. The values are given in micro Tesla. They can be changed while the program is running. Also, there is an array named "Direction Corrections" that enables a software-wise accounting of bad wiring, e.g. if the plus and minus pins of a cable are swapped. Therefore, the entries of this array should be either -1 for swapped pins, 0 for directions where no output is desired or $+1$ when the wiring is fine.

As soon as all the parameters are set, the program can be started with the white arrow on the Lab View panel. Stopping the program is done by pressing the "STOP" button in the interface. This then stops the readout of the sensors and provides an output voltage that is zero. Aborting the program with the red circle on the Lab View panel will stop the sensor readout, but the output voltage will remain on the same level as they were in the last iteration. **In order to set the output to zero it is therefore important to stop the program in the user interface.**

Further on there are parameters that can be changed which are important for the tasks (not visible in Figure 12). They define the physical channels of the voltage in- and outputs, how many samples in which mode and at which rate should be read and the task names. It is suggested that the readout mode is "Finite Samples", the rate is set to 1000 samples per second and channel and 100 samples per channel are read out. The voltage limit is 6 V, and the output limit should be 5 V such that the circuit wont be harmed.

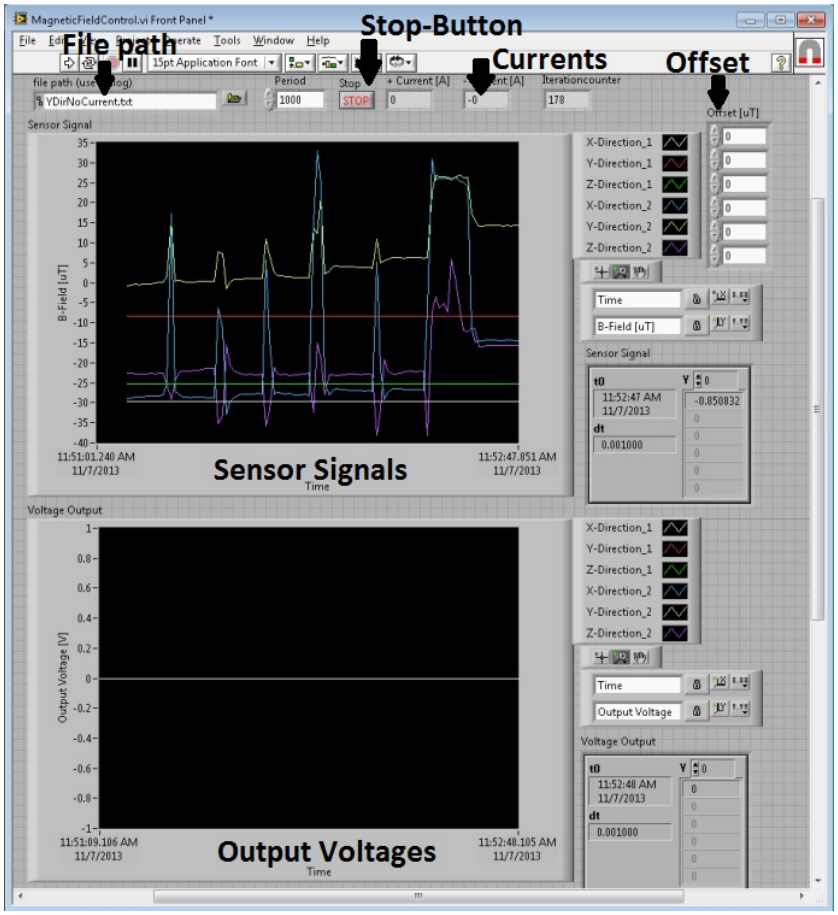

Figure 12: The front panel of the Lab View program for the magnetic field control. The two wave charts display the magnetic fields and the output voltages.

Errors When running the program there is so far only one error that occurs. Always at 10:03 (both, a.m. and p.m.) the connection to the output card is lost. This does not stop the program from running, the sensors are read out just as normal. But the recording of the data is stopped and the output voltage is set to zero. Up to this point it is not really clear what causes this disconnection. It was checked that it is not a possible reset of the router or reassignment of the IP address of the output card. A network traffic activity analysis around the suspicious time has not revealed much, just that the router has problems addressing the card and vice versa. The implemented trouble shooter VI was not able to solve the problem by trying to reconnect to the cards as soon as a connection error occurred.

A possible solution is to make the communication between the computer

and the output card based on VISA sessions, instead of trying to have a stable long term connection. Using VISA sessions has the advantage that every time two devices communicate with each other a new connection is established and closed again as soon as it is no longer needed. This could circumvent the problem mentioned above.

The program is described in more detail in Appendix C where also pictures of the VIs and sub-VIs can be found.

4.4 The Output Card

The output card receives a digital signal encoding the desired output voltage from the Lab View program. A digital to analog converter in the card then produces an analog voltage. The card used here is a NI 9264 analog output card [16]. It has 16 channels, each with a 16-Bit digital analog to converter that can produce voltages up to $\pm 10\,\mathrm{V}$. The voltages produced here will then control the VCCS.

4.5 The Voltage Controlled Current Source

Challenges for the Circuit Design One of the problems faced when attempting to build a control for the magnetic field is that one does initially not know in which direction the magnetic field will point. Also, the direction of the magnetic fields may change over time as the magnets in the neighboring labs are being ramped. Therefore, it is primarily unknown in which direction the current needs to flow through the coils and thus it is important that the device is able to provide a current in both directions.

This enforces special designing for the current source since a zero-crossing is challenging if the sources need to work properly for low but also for higher currents (about 4 A at 8 V) in both directions. There are commercially available power sources that are able to do this, for example four quadrant dc current sources (or also special two quadrant dc current sources) [17] [18]. If one had six such current sources one could drive each coil individually. A downside is that voltage controlled 2- or 4-Quadrant current sources cost at least 3'000 CHF, making a total of more than 18'000 CHF which is clearly too expensive just for a simple control of magnetic fields.

Another possibility to realize such a system is to use only two dc 1-quadrant current sources and design a voltage controlled current source (VCCS) for each coil. All six VCCS are in parallel and are fed by the two dc current sources for the two different directions of the current, Figure 13. They regulate how much current of which source (the positive or negative current source) will flow through the respective coil. An advantage hereby

is that for example the positive current source can provide positive current through four of the coils while the negative current source provides current through the other two coils. Like this, the costs for the circuit are more than an order of magnitude lower than with the version before.

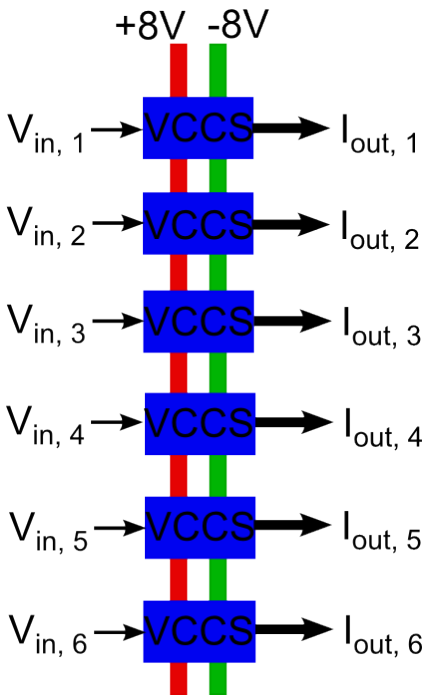

Figure 13: The six voltage controlled current sources are in parallel. They use the same current sources at +8 V and -8 V respectively. Depending on the input voltages, V_{in}, they yield different output currents I_{out}.

Requirements The task of the VCCS is to take the voltage of the output card of the computer, ranging from $-10\,\mathrm{V}$ to $10\,\mathrm{V}$, with no current flowing, and control a current which is proportional to this output voltage, ranging in magnitude from $-4\,\mathrm{A}$ to $4\,\mathrm{A}$. Further important parameters are the resistance of the coils, of $R_C \approx 2\,\Omega$, defining the required voltage of the two dc current sources to $\pm 8\,\mathrm{V}$, depending on the direction of the current. First, the circuit for only one amplifier is explained and afterwards it will be discussed how six amplifiers are connected.

The basic idea is to use the output voltage of the card to control an operational amplifier (OP-AMP) which in turn controls four transistors in two Darlington configurations. These then control a current flowing through

the coils according to the applied output voltage, Figure 16, and feedback to the OP-AMP. In the following the circuit is explained step by step.

The OP-AMP has an inverting input with voltage V^-, a non-inverting input with voltage V^+, and one output. The output voltage is $V_{out} = A_{OL} \cdot (V^+ - V^-)$, where A_{OL} is the open-loop gain of the OP-AMP. It needs to be supplied with a voltage of $\pm 15\,\mathrm{V}$. The outputs always needs to be connected to one of the inputs, although it does not need to be connected directly. The OP-AMP always tries to equilibrate the voltage of its two inputs. If there is for example a voltage divider between the output of the OP-AMP and its inverted input, the OP-AMP will output a voltage that is higher than the voltage in its first input in order to reach the same voltage on the second input as on the first. In our case the voltage from the output card is applied to the non-inverting input. The output controls a Darlington pair such that current flows through the coils and pulls the voltage at the inverting input of the OP-AMP onto the same level as the voltage on the non-inverting input. This will lead to an equilibrium situation. The OP-AMPs used are of the type OP 07 CP.

A Darlington Pair [19] consists of two NPN (or PNP) bipolar transistors which are connected as shown in Figure 14. If there is no voltage V_{in} against ground applied at the first (non-inverting) input port of the OP-AMP there will be no output voltage at the OP-AMP, as the second input of the OP-AMP is pulled on ground potential via the resistor R. Also, the transistors are not conducting which means that there is a high resistance between the $+8\,\mathrm{V}$ port of the current source and the second input of the OP-AMP. Thus no current will flow through the load (here the inductor L). So if there is no voltage V_{in} applied the structure is in the off-state.

If a voltage $V_{in} > 0\,\mathrm{V}$ is applied, the OP-AMP will rise its output voltage (because the two inputs are now on a different potential) and therefore lower the resistance of the first NPN Transistor (NPN 1 in Figure 14). Thus, the potential at the emitter of the first and at the base of the second transistor (NPN 2) is now also finite. As a result the second transistor will also have a lower resistance, and some current will flow, raising the potential at the emitter of the second transistor until it is equal to V_{in}. In this equilibrium state a current will flow from the current source through the second NPN transistor, the inductance (coil) and the resistance R to ground. Note that there will almost be no current flowing through the first transistor as its emitter has more than a $1\,\mathrm{k}\Omega$ resistance to ground (assuming the base-emitter current of the second transistor is small). The resistance of $1\,\mathrm{k}\Omega$ is required

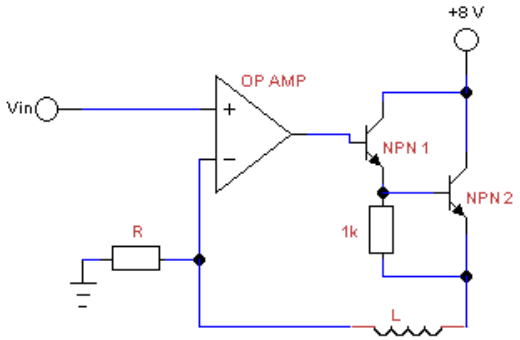

Figure 14: The circuit diagram of the underlying amplifier. The OP-AMP controls the Darlington pair of NPN transistors in order to equilibrate the voltage on its two input ports.

such that charge may flow away from the base of the second transistor.

A Darlington pair is more useful than just one power transistor because a Darlington pair has a very high current amplification (100-1'000) compared to a power transistor (5-10), depending on the device used. This is because small signal transistors have a much higher amplification than power transistors, and the amplification B of the Darlington pair is approximately the product of the amplifications of the two transistors, B_1 and B_2, so $B \approx B_1 \cdot B_2$ [20]. The amplifications are characteristic for the transistors used. Therefore it is more useful here to work with a Darlington pair as the input current is small.

The Resistance R can be determined from the requirements for our circuit. Again, we need to have a current of $I = 4\,\mathrm{A}$ when $V_{in} = 10\,\mathrm{V}$ is applied. Equivalently we can say that there is also a potential of $10\,\mathrm{V}$ on the inverted input of the OP-AMP. Therefore, with Ohm's law we get that

$$R = \frac{V_{in}}{I}. \tag{6}$$

Inserting the values for V_{in} and I we get that $R = 2.5\,\Omega$. Choosing R alike, the amplification stage in Figure 14 works as desired for positive values of V_{in}.

Negative Voltages V_{in} need to be handled by the circuit as well. As described above, the direction of the magnetic field may change over time, and the circuit needs to account for this too. The idea here is that we take another current source that provides a current in the opposite direction to the

source for positive voltages V_{in}. To regulate how much current should flow we again use a Darlington pair, but this time with different polarity than before, as this current source will be on a potential of $-8\,\mathrm{V}$. The PNP-Darlington Pair will thus work likewise as the NPN, just with negative Voltages instead of positive ones. Plugging this together, Figure 15, the circuit now converts voltages from -10 to $+10\,\mathrm{V}$ to currents from -4 to $+4\,\mathrm{A}$.

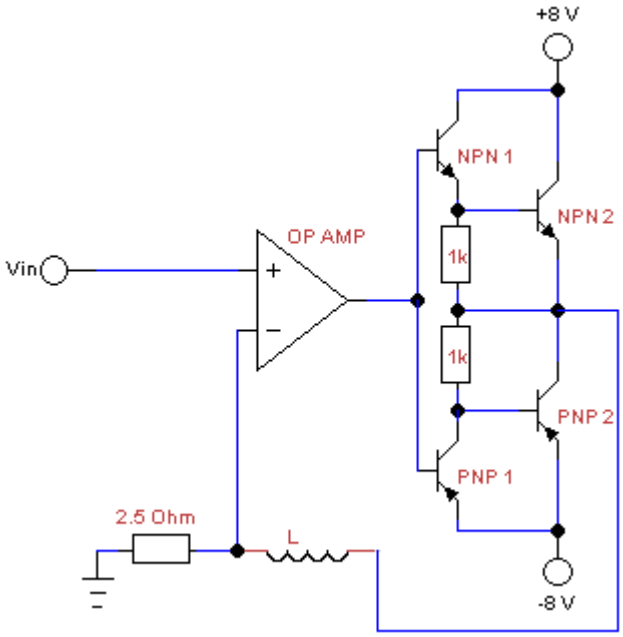

Figure 15: The diagram of the circuit with two Darlington pairs. This circuit is able to convert positive and negative voltages to currents in different directions.

Further Adjustments need to be made to get a better impulse response. For example an oscillating behavior of the circuit output is not desired. Therefore, capacitors from the current sources to ground are necessary, enabling faster switching from low to high currents, as charge is stored in them. They need to have a high capacitance since the currents are strong. Also, there need to be capacitors to ground on the bias lines of the OP-AMP which smoothen fast current peaks in case of a voltage peak of the input voltage V_{in} to ground. Also, these capacitors smoothen out noise in the voltage bias.

A further change to the circuit design is made considering the frequencies at which the setup is operated. As the power sources used are not switching

at high speed, there is no point in allowing the input signal to have high frequency components. Otherwise we introduce noise in the circuit. Therefore, a low-pass filter is set in front of the first input of the OP-AMP. The cutoff frequency is chosen to be at $\approx 2\,\mathrm{Hz}$.

To obtain an estimation of the power P that will be dissipated in the resistor with $2.5\,\Omega$ we calculate

$$P = R \cdot I^2.$$

In the worst case of $I = 4\,\mathrm{A}$ flowing a power of $P = 40\,\mathrm{W}$ is dissipated. This is a problem, because it requires a special kind of resistor that is able to handle such powers, and also needs to be cooled. As the current needs to be $4\,\mathrm{A}$ one can only circumvent this problem by reducing the resistance R e.g. to $0.25\,\Omega$. This again requires the voltage V_{in} to be $\pm 1\,\mathrm{V}$ at maximum, Equation (6). This can be realized by using a voltage divider that reduces the input voltage to one tenth of the initial value. The power dissipated will thus be reduced by a factor of 10, which leads to a dissipated power of $4\,\mathrm{W}$, and can be handled by normal wire resistors without further cooling.

The voltage divider is chosen to be of high resistance, $90\,\mathrm{k}\Omega$ and$10\,\mathrm{k}\Omega$ respectively, such that the output power of the NI card is reduced. With the cutoff frequency f_C of

$$f_C = \frac{1}{2\pi RC} \approx 2\,\mathrm{Hz}$$

a capacitance of $\approx 1\,\mu\mathrm{F}$ for the capacitor of the low-pass filter is needed. Note that the voltage divider and the low-pass filter share the $90\,\mathrm{k}\Omega$ resistor. The diagram of the final circuit is shown in Figure 16.

One should check whether or not it makes sense to include fly-back diodes into the circuit such that it can be protected against induced voltage peaks as it is usually the case for coil current supplies. In this case it is not needed since first, if one includes diodes into the circuit, they will immediately shunt the current sources as soon as the output voltage of the OP-AMP is $\neq 0$. Second, the induced voltage $V_{induced}$ is small, since

$$V_{induced} = L \cdot \dot{I}.$$

The inductance L of the coil can be estimated as follows: Assuming the coils to be ring-shaped, and using the expression

$$L = N\mu_0 r \cdot \left(\ln\left(\frac{8r}{a}\right) - 2\right)$$

for the inductance of a wire loop of radius $r = 0.3\,\mathrm{m}$ with wire radius $a = 0.5\,\mathrm{mm}$ and $N = 30$ windings we get that $L \approx 75\,\mu\mathrm{H}$ [21]. We estimate

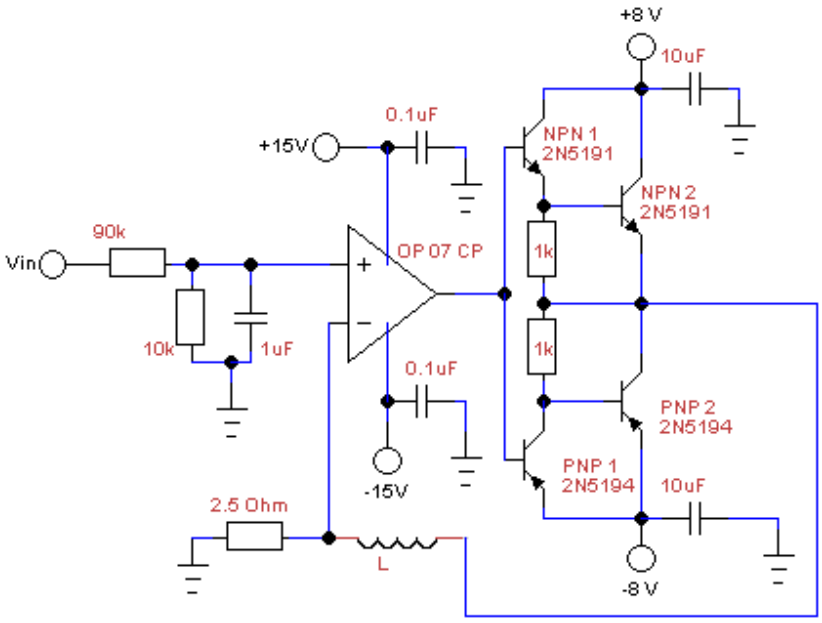

Figure 16: This diagram shows the circuit how it is actually implemented and the parts used. The low-pass filter and voltage divider are in front of the OP-AMP, which then controls two Darlington pairs. These in turn regulate the current through the inductive load L which then flows to ground via the 0.25Ω resistance.

$\dot{I} \approx \Delta I/\Delta t$. The rise time of the current is on the order of $\Delta t \approx 15\,ms$, compare Figure 21. The maximum current difference is $\Delta I = 4\,\mathrm{A}$. Finally we obtain

$$V_{induced} \approx L \cdot \frac{\Delta I}{\Delta t} \approx 75\,\mu\mathrm{H} \cdot \frac{4\,\mathrm{A}}{10\,\mathrm{ms}} = 30\,\mathrm{mV},$$

which is a very small value, and thus it is unlikely that the circuit could take any damage of inductive effects.

A PCB (Printed Circuit Board) is a plastic slab that is on both sides coated with copper (usually $35\,\mu$m thick). The copper coating can be milled or etched away such that the wiring of the circuit is directly on the plastic board, and just the circuit elements need to be added and soldered to the PCB. Such a PCB was designed because this reduces the effort to wire the circuit drastically and it is much more compact. The design files (the top and bottom layer) are shown in Figure 17. The design was made in Eagle, a special PCB design program. This tool can be run with a free-ware license, limiting only the size of the PCB. As the PCB designed here was bigger than

the size allowed by the free-ware license, access to a full license was enabled by Martin Gähwiler of the Elektronik Lehrlabor at ETH Zürich.

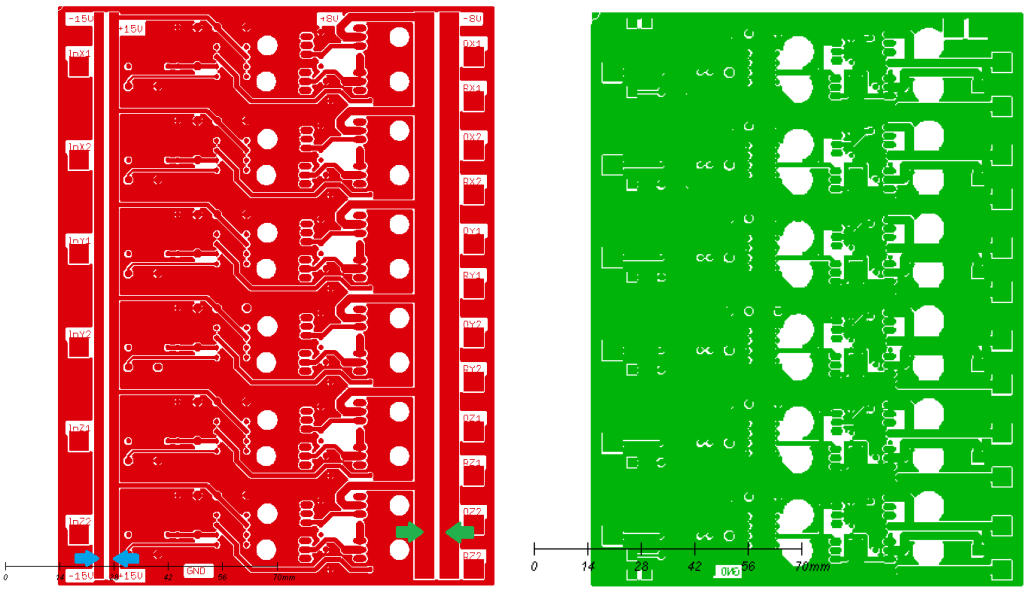

(a) Top layer of the PCB. The lines to the left are the voltage lines (blue arrows), the lines to the right (green) conduct the current. The ports are rectangular pads.

(b) The bottom layer of the PCB. The big white areas are where the transistors will be screwed to the PCB. Most of the bottom layer belongs to the ground plane.

Figure 17: Top and bottom layer of the PCB-design. Colored areas indicate remaining copper, white areas indicate where the copper is milled away. The amplifiers are in a row next to each other.

In the PCB designed, six VCCS are mounted in parallel, sharing common supply voltages ($\pm 15\,\mathrm{V}$) for the OP-AMPs and current sources (which operate at $\pm 8\,\mathrm{V}$). Each VCCS has an input (the pads on the very left side of Figure 17a), an output port for the current and a return port (both on the very right side of Figure 17b), such that the coil can be wired in-between.

Things that are important to respect during the design are that the current lines (wires on the PCB that carry a lot of current) need to be thicker than voltage lines, as heating may occur if the wires are too thin. An on-line tool [22] was used to get an estimation of the wire thicknesses required. Also, the transistors were ordered to be on one line, such that a cooling element can be mounted easily.

The designs were then sent to the Bastli [23] where the PCB was produced. The bare PCB (Figure 18) was assembled by hand. This process

took a bit more than a day, and the result is shown in Figure 19. The white paste on the transistors visible to the very left is heat conduction paste that ensures a good heat exchange between transistors and cooling elements.

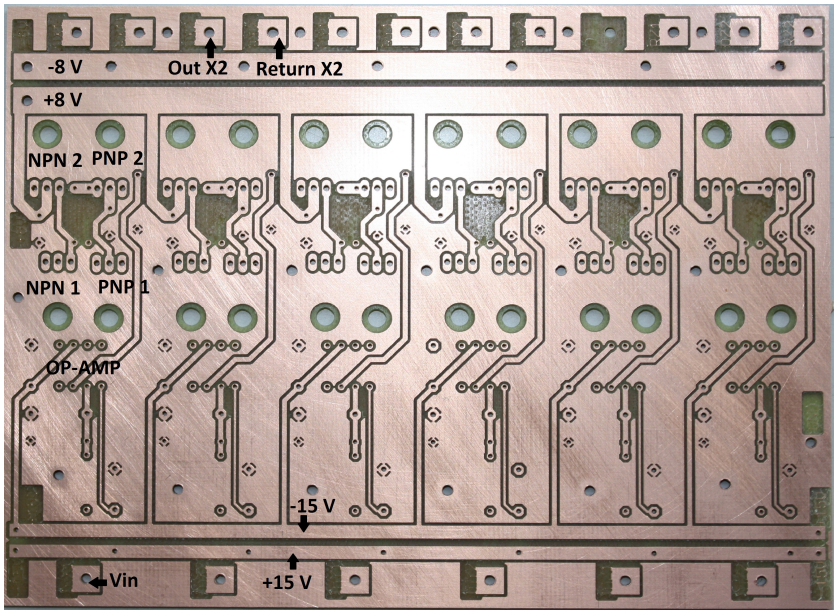

Figure 18: Top view of the PCB. The holes in the board are used to put the legs of the elements through and contacting the top with the bottom ground plane. Right beneath the lower series of big holes for the transistors the OP-AMPs will be placed.

Very careful soldering is important, as else there might be cold soldering joints that lead to improper behavior of the whole circuit. So, it is important that enough soldering tin is used to ensure a proper and solid connection. If it has to be removed again, the soldering braid may loose some of its (very fine) wires which may shunt the circuit. Finding such an error is very tedious work because the error could be in any of the six amplifiers. A short summary on how to find errors in case of a failure of the circuit is given in Section 5.

The PCB design works as desired, there are no design errors. Still, it could be improved in a way that no wires run beneath the OP-AMP. These are rather hard to connect to the legs of the OP-AMP which in turn is one of the parts of the circuit that is rather likely to fail when the circuit is improperly handled and therefore might require replacement.

The Housing is made of a commercially available chassis. Holes were drilled into it such that the PCB can be mounted on screws through the

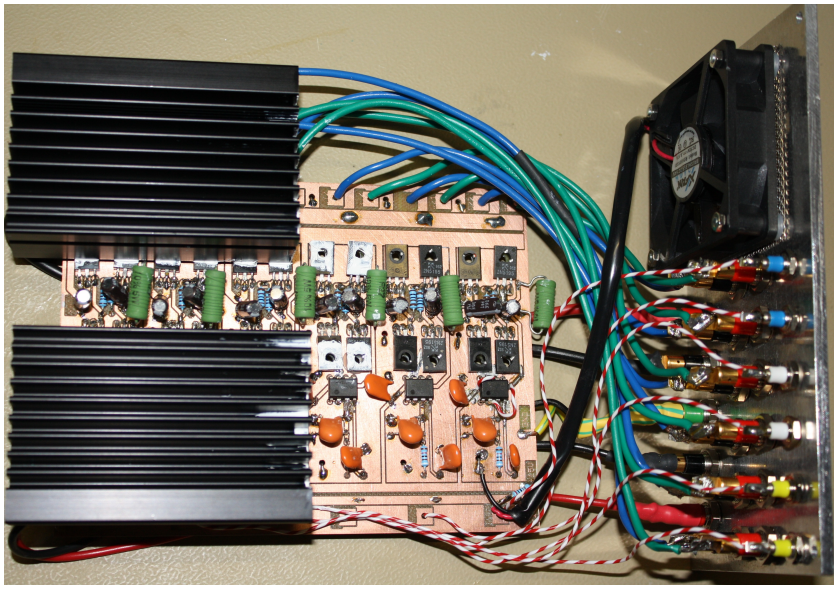

Figure 19: In the middle part of the picture the assembled PCB is visible, showing the different elements. The black structures on the left are cooling elements, and on the right the wiring with the back side of the front plate is visible.

chassis. The front plate of the housing has 23 plugs, 2+2 for the voltage- and current-supply, one for ground and 18=6·3 for the six coils (one for the voltage input, and two such that the coil can be wired, Figure 20a). The plugs belonging to one direction are ordered in columns. Also, a fan is mounted such that the heat can be transported away from the cooling elements. The correct wiring of the apparatus is described in Section 5.

Characterization of the Circuit It is interesting to have a look at the performance of the circuit that was built. An important quantity is the rise time of the voltage that the VCCS outputs upon a pulse as an input, Figure 21, since this limits the performance on the hardware side. An arbitrary waveform generator was used to apply pulses to the VCCS. Connecting both, the pulse generator and the circuit output to an oscilloscope one can compare the output voltage to the applied pulse. The impulse answer on a $+2\,\mathrm{V}$ square pulse, Figure 21a, yields a rise time of $\approx 15\,\mathrm{msec}$. The rise time of the output voltage upon a $-2\,\mathrm{V}$ pulse is $\approx 25\,\mathrm{msec}$, Figure 21b. This difference in the rise time is because different transistors are used for the positive and negative current control, and they do not behave identically. Note that there is no

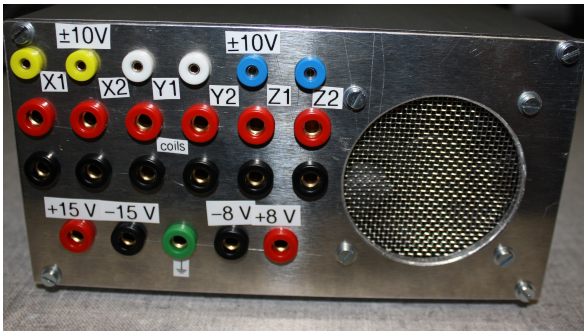

(a) The front view of the housing. The plugs in the first row are for the input voltages, the plugs in the second and the third row are for the wiring of the coils. The last row is for voltage-, current-supply and ground.

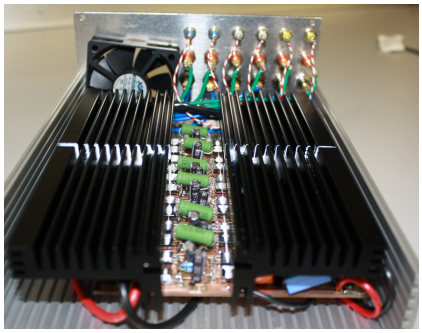

(b) This is the view from the rear with open housing. The cooling elements are the black parts, the green elements are the 0.25 Ω resistors.

Figure 20: The housing shown from the front (a) and back (b) without cover.

oscillatory behavior of the circuit, just an exponential increase of the output voltage towards the final value.

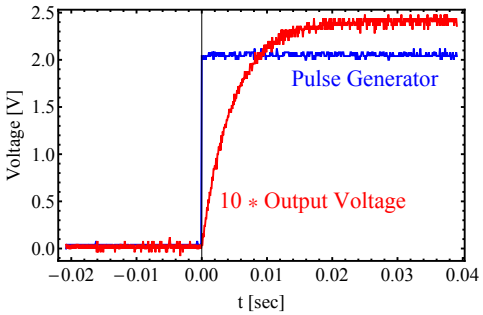

(a) The impulse response of the VCCS upon a +2 V square pulse.

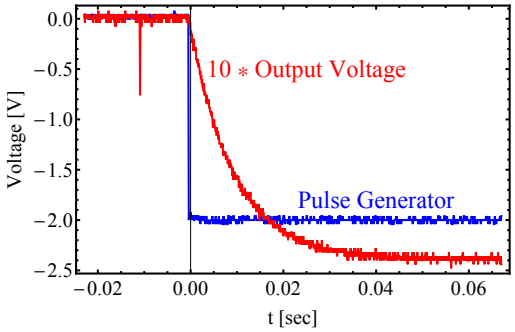

(b) The impulse response of the VCCS upon a −2 V square pulse.

Figure 21: Pulse responses of the VCCS. The output voltage is measured across the Out port (Figure 18 of channel X2, the different channels behave similarly. Note that the values for the output voltages are ten times smaller than indicated on the plots.

It is not entirely clear why the rise time of the voltage is so short - the low pass filter should decelerate the rate. A possible reason for this is that the pulse generator lowers its output impedance automatically such that it can provide the pulse. This means that a large current would flow and saturate the capacitor of the low pass filter, therefore disabling it.

The zero-crossing of the circuit is also of interest, since a change of the

direction of the magnetic field could occur. In Figure 22 a saw-tooth function was applied to the circuit, and the response of the circuit was measured. As the timescale is on the order of milliseconds, the OP-AMP and the transistors have enough time to react on the applied voltage change, and there is no "kink" in the zero-crossing. This is advantageous, because it means that the feedback will be able to account for small corrections around zero magnetic field. Figure 22b shows a detailed view around a zero-crossing, note the altered scale. There is a time-delay of $\approx 10\,\text{msec}$ of the output voltage with respect to the applied pulse. But this does not matter in the application of the device here as we are not interested in quick changes.

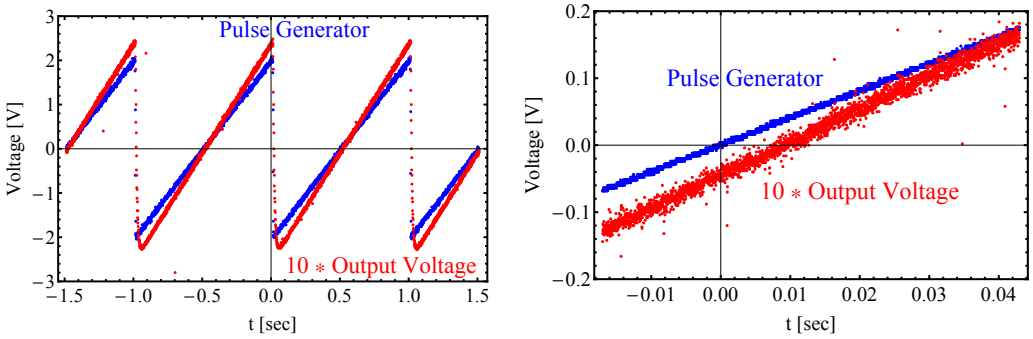

(a) The response of the circuit to an applied saw-tooth pulse with a frequency of 5 Hz and a peak-to-peak voltage of 4 V. The symmetry of the pulse is 100%.

(b) A close-up view of the zero-crossing. The output voltage is slightly delayed, but there is no anomalous behavior. Note the different scales and axes origins.

Figure 22: The zero passing of the output voltage is observed. The output voltage is measured at the Out port (Figure 18 of channel X2, the different channels behave similarly. Note that the values for the output voltages are ten times smaller than indicated on the plots.

The scaling of the output current with the applied voltage was not measured in detail. A quick check revealed that the current scales about linearly with the voltage, such that $\approx 3.7\,\text{A}$ will flow as 10 V are applied on the input. All in all we can therefore state that the circuit behaves as required.

4.6 Characterization of the Feedback

The performance of the whole device needs to be characterized as well. The setup is such that the two sensors are placed inside the cube. Sensor 1 is close to coils X1, Y1 and Z1 and analogously for sensor 2. Note that the amplifier for the Z2 coil did not work at the moment when the traces were recorded, so that the Z2 coil was just wired in series to the Z1 coil. This also shows

the advantage of a differential measurement with respect to a non-differential setup, as discussed in Section 3.4.

Switching the Feedback On In Figure 23 it is shown what happens to the values of the sensors when the feedback is turned on. Figure 23a shows the field amplitudes at the sensor positions on a normal scale (the Z2 field amplitude is not visible since it is higher) and one can see that as soon as the feedback is turned on at $t = 0$ the field amplitudes drop and stabilize around $B = 0\,\mathrm{T}$. They tend to overshoot, but do not oscillate, so it seems as if they are critically damped. Figure 23b is a logarithmic plot of the absolute value of the field amplitudes. Between seconds 30 and 90 a clear exponential decrease of the field strength is visible.

The fit shown in Figure 23b is of the form $a \cdot \exp[-k \cdot t]$ with the parameters $k = 0.0686\,\mathrm{s}^{-1}$ and $a = 1.409$. The exponential decay is expected for an integral controller for an initial deviation from the set-point. The time constant $\tau = 1/k = 14.5\,\mathrm{s}$ is a result of the parameters of the integral control (update rate and increment factor 0.5).

The fluctuations after second 100 are due to the fact that the threshold of the control program is reached. The dips in the field strength are due to zero crossings. The behavior of the Z1 direction is worse than the behavior of the others because the Z coils have less windings and are bigger than the other coils, leading to a lower inductance and higher sensibility to crosstalk from other coils.

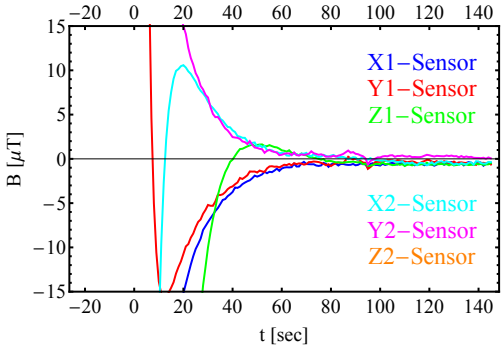

(a) The magnetic field when the feedback is turned on. One can see that it looks as if the feedback is critically damped.

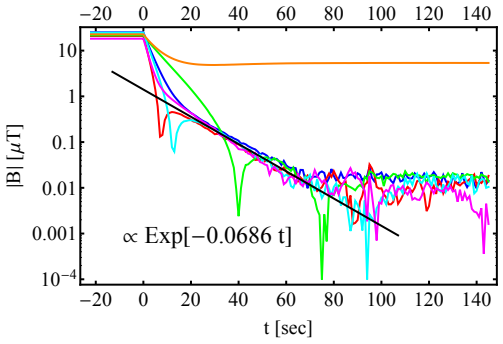

(b) A logarithmic plot of the absolute value of the magnetic field. The dips origin from a zero crossing.

Figure 23: The magnetic field over time. Initially there is no feedback, the sensors are just measuring the external field. Then, at second 22 the feedback is turned on. The Z2 feedback does not work, the current through the two coils is z-direction is the same and determined by the Z1 Sensor signal.

It is important to note that the field strength shown in Figure 23 is so low only at the position of the sensors. In order to get a field that is essentially vanishing in the middle of the Helmholtz cube, calibration is needed. Then, an offset can be applied to account for the deviations of the field strength at the sensor positions with respect to the center of the cube. This is of course not entirely easy to do in a very precise way, so therefore one can not expect the magnetic field in the center of the cube to be as low as one hundredth of a micro Tesla for the whole volume of the experiment. But it should be possible to reduce the magnetic field to at least $1\,\mu$T everywhere.

The time required to get to a field strength that is lower than $1\,\mu$T can be estimated to be about 20 seconds. To reach $0.1\,\mu$T, 40 seconds are required. If the coils are poorly aligned this might change as crosstalk between the coils delays the control.

Compensating a Ramping Magnet In the traces shown in Figure 24 it is visible what happens if the magnet of the Wegscheider-Group is ramped. It was initially at 0 T, and was then ramped up with 0.3 T/min to 2.1 T, and after ≈ 3 min ramped down again. Figure 24a shows the change of the output voltage over time when the magnet is ramped. The resulting change in the magnetic field strength, Figure 24b, is below $0.1\,\mu$T. But it can also be seen that the change indeed has an influence, and the value of the magnetic field is always deviated away from 0 as the field is still changing. This is because the update rate is only 1 Hz: the rate of change of the magnetic field when the magnet is ramping is (data from Figure 5)

$$\frac{\mathrm{d}B}{\mathrm{d}t} \approx \frac{\Delta B}{\Delta t} = \frac{\sqrt{8^2 + 26^2 + 16^2}}{2400} = \frac{32}{2400} = 13\mathrm{nT/s}.$$

This means, that the deviation in Figure 24b can roughly be explained by the limited update rate.

This happens because the controller used is not a full PID-controller [24], but just adds up the error signals of the past (it's just an I-controller). If a controller that includes a differential part was implemented, this behavior could be suppressed. Also, one could lower the effect by a faster update rate.

The Field with Compensation The last characterization of the feedback is the measurement of the field inside the coil cube when the feedback is tuned on. As there are only two magnetic sensors available it was not possible to measure the field with running feedback. This problem was circumvented by turning on the program and fixing the output voltages as soon as a steady state was reached. The feedback was turned off while the output voltages

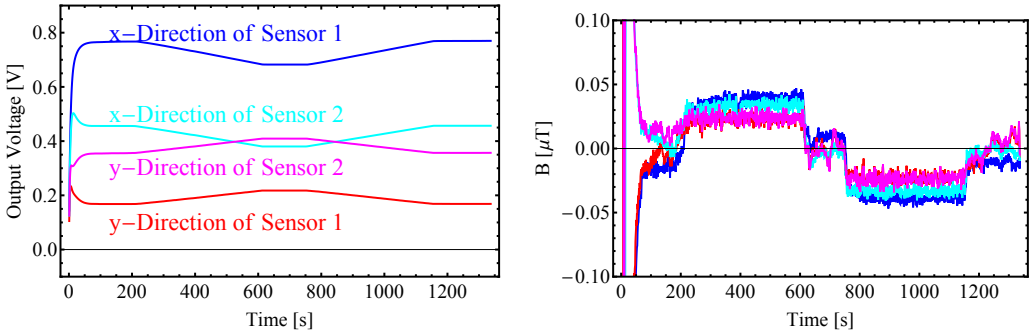

(a) The change of the output voltage to the VCCS when the magnet of the Wegscheider-Group is ramped and the Feedback is on. It is clearly visible that the feedback reacts to this distortion.

(b) The field at the position of the sensors when the magnet of the Wegscheider-Group is ramped and the Feedback is on. The field is always below 50 nT, but a constant offset can be seen.

Figure 24: Output voltage and sensor signals when the magnet of the Wegscheider-Group is ramped and the Feedback is on. Clearly the Feedback reduces the magnetic field in the coil cube.

still applied to the VCCS. Like this, the same field as with the feedback being turned on is obtained. Then, one of the sensors was used to measure the field inside the cube, Figure 25.

The fields in x and y-direction are reduced to a level below $2\,\mu$T respectively $1\,\mu$T. The field in z-direction has a finite and approximately constant gradient, this is because the Z-coils are wired in series, and a differential compensation is not possible. From this curve the advantages of a differential setup are clearly visible, especially if we compare the characteristic size of the compensated area. The errors in Figure 25 arise from an imprecise positioning of the sensor and bad alignment. This figure shows that the feedback works and compensates the magnetic field inside the coil cube down to few micro Tesla. This could be improved introducing an offset.

5 Brief Manual

In the following, fist a short introduction on how to wire the apparatus is given. Afterwards some possible error schemes are discussed and standard solutions provided.

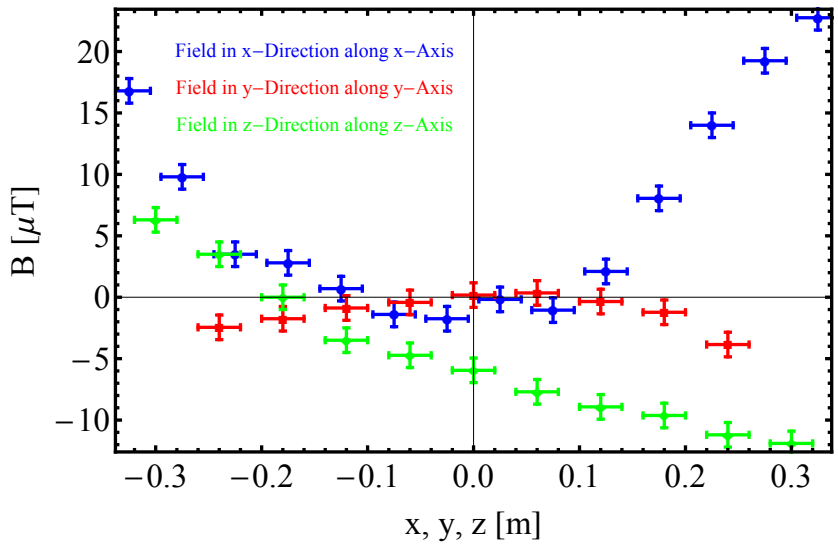

Figure 25: The field inside the coil cube when the voltages obtained from running the feedback are applied. The fields are measured in the direction of the axis of the respective coil pairs.

5.1 Wiring the Apparatus up

The Voltage Source needs to be set on 15 V. The +15 V port needs to be connected both to the amplifier and the + port of the Suco-Box with the 275 Ω resistance. The latter will power the magnetic flux sensors. The -15 V port needs to be connected to its corresponding part on the amplifier. The COM port of the voltage source needs to be connected to the mass of the voltage source, to the ground of the Suco-Box and the ground of the amplifier. When running, the current should display a value of ≈ 200 mA.

The Current Sources need to yield a potential with respect to a common ground. Thus, the + port of source 1 needs to be connected both to the - port of source 2 and to ground at the amplifier (and therefore also to ground of the voltage source). Then, the - port of source 1 needs to be connected to the -8 V port of the amplifier, and the + port of source 2 needs to be connected to the +8 V port of the amplifier. Both current sources need to give an output voltage of 8 V, the current limit should be set to 4 A.

The coils have an in- and an output. Wire them according to the color code and the direction names. The corresponding plugs of the amplifier are in the second and third row. It is important to place the coils in such a way that

the magnetic field produced by a positive current points in the same direction for both coils in the same spatial direction (e.g. both X-coils should yield a field pointing in x-direction when a positive current flows through them).

The Succo-Box just contains a resistance of 275 Ω on the positive voltage line and a connection to the ground on the other side on the ground line. The 275 Ω resistor acts as a voltage divider to power the magnetic flux sensors which need 6 mA at 12 V. Connect the ground of the Succo-Box to the ground of the voltage source and the +15 V input port to the +15 V port of the voltage source. The BNC output of the Succo-Box needs to be connected to the BNC input of the sensors.

The Sensors need to be supplied with 12 V and 6 mA. This supply they get from the BNC output of the Suco-Box. The simple wires need to be connected to the NI analog input card. The wire labeled with "X1" should go to AI0, "Y1" should go to AI1, and so on, and "X2" goes to AI3. If this sequence is changed, corresponding changes in the Lab View-program need to be made (changing physical channels of the reading tasks). Note that the ground of the sensor signal is the only ground at a different potential than the ground of the voltage source.

The Input Card must be connected to the sensors as described above. Of course, it also must sit in the NI card chassis which in turn needs to be connected via LAN to the computer running the Lab View program.

The Output Card needs to be connected with the special cable with the mini-banana plugs on the one and to loose wires on the other ends. Again, connect the loose wires in the same sequence as the sensor wires (or else change the physical channels of the output task in Lab View). The mini-banana plugs need to be connected to the corresponding ports at the amplifier. Also, connect the ground with the ground of the amplifier. The NI card chassis needs to be connected via LAN to the computer running the Lab View program.

All the circuits need to be closed when the amplifier is connected to the voltage- and current sources. If there are open circuits (e.g. coils are not connected) no feedback to the OP-AMP will be possible and hence a lot of current will flow, potentially damaging the amplifier. The circuit can also be run if the in- and outputs for the coils at the amplifier are directly connected with a wire (shorted).

5.2 Error Handling

A current source shows "OUP" This is the overload protection mode of the current source. Most likely one or more coils are not properly connected. If there are open loops in the circuit, the OP-AMP wont get a feedback and just open a Darlington until 4 A will flow.

One direction only yields a current of 7 mA In this case the power conducting transistor of this direction does not work any more, and just transistor 1 (in Figure 14) conducts current ($8\,\mathrm{V}/1\,\mathrm{k\Omega} \approx 7\,\mathrm{mA}$). This means that the box has to be opened and the corresponding transistor needs to be replaced.

The feedback does not work This can be due to the Boolean "Create Output" in the block diagram view of the Lab View program is turned off.

6 Outlook

So far, the device is operating properly. Of course, as soon as it is used to shield magnetic fields around the experiment, careful calibration is needed. This can be done using the position of the electron beam and deviating it by applying an offset and comparing where on the MCP it is detected. In order to improve the system described so far one can still work on several things:

- The coils can be improved such that a more homogeneous magnetic field can be achieved and less current is needed to supply a magnetic field of the desired strength. In Appendix B some estimations for different coil configurations are given.

  For the connection to the coils it is strongly recommended to take plug sockets that have at least a diameter of 4 mm, smaller plugs will easily break off. This can lead to a damage on the VCCS because if there is no feedback any more the current will increase to the maximum and possibly overheat a transistor.

- A PID control can be integrated into the Lab View program, such that a quicker response to varying fields can be achieved, see Section 4.6. With a PID control situations where the field is too large over long time although the change is constant, as in Figure 24b, can be avoided.

- The program should be included in the logger program of the experiment.

- Also, it would probably be useful to optimize the data handling of the sensor value data. For example it would make sense to take the average over a well-distributed set of samples when reading in the sensor signal, and not just the 100 last samples. Like this, one could probably lower the threshold in the program without worsening the stability of the system.
- Fuses could be integrated to the circuit, such that it is no longer as fragile as it is at the moment.
- Provided that coils with a higher inductance are available, one could integrate the whole circuit with current- and voltage-supply in one housing, reducing space requirements and cable spaghetti.
- The 10:03-connection-loss-bug mentioned in Section 4.3 needs to be fixed in order to ensure continuous running. This could be done using VISA sessions.
- It should be thought about running the current sources on a voltage of only 6 V. This might have the advantage that the transistors are not burnt immediately as soon as the feedback to the OP-AMP is lost.

7 Acknowledgment

I would like to thank Tobias Thiele for helping me whenever I got stuck during this project and providing me with valuable advice. I enjoyed working with him a lot since usually solutions were found quite quickly. Stefan Filipp helped me a lot with the Lab View programming. Also, I would like to thank Martin Gähwiler from the Elektronik Lehrlabor for helping with the design of the circuit of the amplifier and giving access to an Eagle license. Special thanks go to Hansjürg Schmutz who took a whole afternoon to help finding problems in the circuit. Of course I would like to thank Prof. A. Wallraff to provide the opportunity of making such a project. Personally, I think I have learned a lot during this time, especially considering electronics and mechanics. Also, I enjoyed the nice atmosphere in the group and many interesting discussions.

References

[1] Feynman, R. P., Simulating Physics with computers, International Journal of Theoretical Physics 21 (6): 467-488. doi: 10.1007/BF02650179, 1982.

[2] V. Bouchiat et al., Quantum coherence with a sinle Cooper pair, Physica Scripa T76, 165-170, 1998.

[3] Cirac, J. I., Zoller, P., Quantum Computations with Cold Trapped Ions, Phys. Rev. Lett. 74 20, 4091-4094 (1995).

[4] Hogan, S. D. et al. Driving Rydberg-Rydberg Transitions from a Coplanar Microwave Waveguide, Phys. Rev. Lett. 108, 063004 (2012).

[5] ACGIH, Documentation of the Threshold Limit Values for Chemical Substances and Physical Agents & Biological Exposure Indices, ACGIH Worldwide, p. 142

[6] J. D. Jackson. Classical Electrodynamics, Fourth Ed. Section 5.15

[7] T. F. Gallagher. Rydberg Atoms, Cambridge University Press, Section 6

[8] Metal Ravne Steel Selector. Steel PK12, http://www.metalravne.com/selector/steels/PK12.html, 26. Nov 2013.

[9] British Stainless Steel Association. Magnetic Properties of Stainless Steel, http://www.bssa.org.uk/cms/File/SSAS2.81-Magnetic%20Properties.pdf, 26. Nov 2013.

[10] J. D. Jackson. Classical Electrodynamics, Fourth Ed. Section 5.12

[11] Sekels, Mu-metal magnetic shielding and shielding foils, www.sekels.com, 8. Nov 2013.

[12] Technische Beratung Ingenieurbüro, Dirk Bunner, http://www.technik-consulting.eu/index.php?cat=Wissenschaft&page=Helmholtz, 15. Nov 2013.

[13] Stefan Mayer Instruments. Miniature Triaxial Fluxgate Sensor FLC3-200, http://www.stefan-mayer.com/flc3.htm, 2. Dez. 2013.

[14] National Instruments, NI 9205 Analog Input Module, http://sine.ni.com/nips/cds/view/p/lang/en/nid/208800, 18. Nov 2013.

[15] National Instruments, LabView, http://www.ni.com/labview, 18. Nov 2013.

[16] National Instruments, NI 9264 Analog Output Module, http://sine.ni.com/nips/cds/view/p/lang/en/nid/208807, 18. Nov 2013.

[17] Heiden Power, 2- & 4-Quadrant Modes, http://www.heidenpower.com/en/products/electronic-loads/33-products/electronic-loads/333-1311-nl-2-4-quadrant-modes.html, 18. Nov 2013.

[18] KEPCO's BOP family of 4-Quadrant bipolar power supplies, http://www.kepcopower.com/1461971.pdf, 18. Nov 2013.

[19] U.S. Patent 2'663'806: Semiconductor signal translating devices, Sidney Darlington.

[20] Ulrich Tietze, Christoph Schenk: Halbleiter-Schaltungstechnik. 12. Auflage. Springer, Berlin 2002, ISBN 3-540-42849-6, page 177.

[21] R. S. Elliott: Ecectromagnetics. IEEE Press, New York 1993. Note that the constant of -3/2 for the uniform current density result is wrong.

[22] PCB Trace Width Calculator, http://circuitcalculator.com/wordpress/2006/01/31/pcb-trace-width-calculator, 11. Nov 2013.

[23] PCB Service of the AMIV Bastli at ETH Zürich, https://pcb.mueslo.de, 18. Nov 2013.

[24] Araki M., PID Control, http://www.eolss.net/ebooks/Sample

[25] The Shop of the Physics Department of ETH Zürich, https://lager.phys.ethz.ch/en/E/

[26] ON Semiconductor, 2N5194 PNP Transistor Data-Sheet, http://www.onsemi.com/pub_link/Collateral/2N5194-D.PDF

[27] ON Semiconductor, 2N5191 NPN Transistor Data-Sheet, http://www.onsemi.com/pub_link/Collateral/2N5191-D.PDF

[28] Texas Instruments, OP 07 CP Precision Operational Amplifier, http://pdf.datasheetcatalog.com/datasheet2/c/0gzhglfo9kzczeqd5oft6g445lpy.pdf

Amount	Part No.	Description
12	30007.11	Transistor bipolar, PNP/2 N 5194/Ic 4000 mA, [26]
12	30007.12	Transistor bipolar, NPN/2 N 5191/Ic 4000 mA, [27]
6	30012.4	Operational Amplifier/OP 07 CP/ Precision, [28]
6	30400.6	Wire Resistor, 5W, 0.27 Ω
6	30381.23	Metal Film Resistor, 0.6W, 91 kΩ
6	30381.1	Metal Film Resistor, 0.6W, 11 kΩ
12	30380.26	Metal Film Resistor, 0.6W, 1.1 kΩ
12	30377.1	Electrolytic radial capacitor, 10 μF
12	30378.1	Dry electrolytic capacitor, 0.1 μF
6	30062.18	Polyester foil capacitor, 1 μF

Table 1: List of the parts required for assembling the PCB.

[29] National Instruments, LabView, Continuous or Finite Sampling Modes, http://digital.ni.com/public.nsf/allkb/B86AA2D2FDE9A16086256FFC00604202

Appendix

A Components needed for the Assembly of the PCB

For the assembly of the PCB only components that are available in the shop of the physics department [25] are used. This makes ordering and replacing broken parts considerably easier. The list of the required parts is given in Table 1. The total costs are CHF 51.60.

Additional parts needed when constructing an entirely new VCCS are:

- Two KO HL 6 combination cases (Part No. 30416.2).
- Two front panel 6+6 (Part No. 30416.5).
- Four self sticking rubber legs (Part No. 30258.1).
- Four cooler profiles, type SK 96 (Part No. 30049.7).
- Screws (M3), washers and spacing elements (of ≈ 15 mm length) to fix the cooling elements onto the PCB and the PCB at the case.
- A fan that fits into the case.

- Resistors dependent on the fan, to create the potential needed to power the fan. Pay attention that the current through fan and resistor matches the requirements of the fan.

- Laboratory plug sockets, depending on the cables chosen.

When assembling the PCB it is very advisable to fist contact through all vias and connect ground, voltage and current supply. Like this, one VCCS after the other can be soldered onto the PCB and tested immediately. Error handling gets much easier as one can always test whether or not the latest VCCS works, knowing that all the previously built VCCS work. However, if this is not done, it gets hard to find errors, as everything is in parallel and it can not easily be determined which VCCS makes troubles.

Also note that it is a bad idea to replace OP-AMPs unless this is absolutely necessary because it will get much more difficult to solder the OP-AMPs as the pads get worn out. Experience tells that the defect part is usually one of the transistors, most likely the power carrying one.

B Comparison of Round and Rectangular Coils

As mentioned in Section 6 a possible way of improving the setup is making better coils. This would be helpful because the current required to get a certain magnetic field could be lowered using coils with a higher inductance. Possible concerns about a loss of precision are causeless because the OP-AMP used is very precise [28].

Better designed coils could also have an advantageous effect on the homogeneity of the field in the target area. A comparison between round coils in a Helmholtz configuration and rectangular coils is given in Figure 26. For the rectangular curves the geometry parameters from above are used again. The round coils have a radius of 0.25 m and differ in the distance between the coils. All coils are assumed to have $N = 30$ windings and a current of 1 A flowing through them.

It is clearly visible that the Helmholtz configuration yields the most homogeneous field along the coil axis. But if the distance between the coils is increased, round coils of the same size do not yield a homogeneous field over a large distance any more. Increasing the the side lengths of rectangular coils makes them to yield a more homogeneous field.

It should be noted that this simulation alone is not enough to decide what kind of coils are best suited to make a homogeneous field at the experiment. Especially important is that this simulation considered only the field along

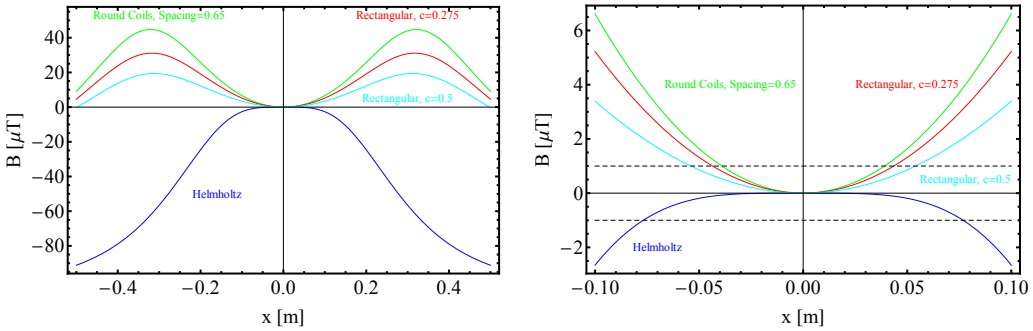

(a) The fields created by coils in a Helmholtz configuration (blue, $R = 0.25\,\mathrm{m}$), by round coils with a distance of $2a = 0.65\,\mathrm{m}$ (green), the rectangular coils we have (red) and rectangular coils with $c = 0.5\,\mathrm{m}$ (cyan).

(b) A close-up of the region around the origin of Figure 26a). The dashed lines indicate a field of $1\,\mu\mathrm{T}$. One can clearly see that the Helmholtz configuration yields the most homogeneous field around the origin. Note the different scale.

Figure 26: Simulation of the fields along the coil axis of different coils. Note that these are effective fields, they are assumed to compensate a constant field such that the magnetic field at $x = 0$ vanishes.

the coil axis, and not perpendicular to it, although the two most important coil pairs will have an axis orthogonal to the direction of the beam.

C Lab View Programs

In the following, the Lab View programs and virtual instruments are shown. The discussion will follow an iteration of the main program, Figure 29.

First, the initialization of the tasks is performed. This includes the names of the tasks and their physical channels. Then the sample clock defining the readout mode is initialized by obtaining the information about the sample mode [29], the readout rate and number of samples obtained by one readout. Also, a file logging the sensor signal and output voltages is created and the maximum input voltages defined. As soon as the initialization is done the first iteration of the loop starts.

One readout step is done in such a way that the readout tasks needs to be activated, then a readout is performed, and the task is stopped again. This is all done using standard DAQmax VIs (data aquisition and measurement automation explorer virtual instruments). After the stopping of the task an error check is performed.

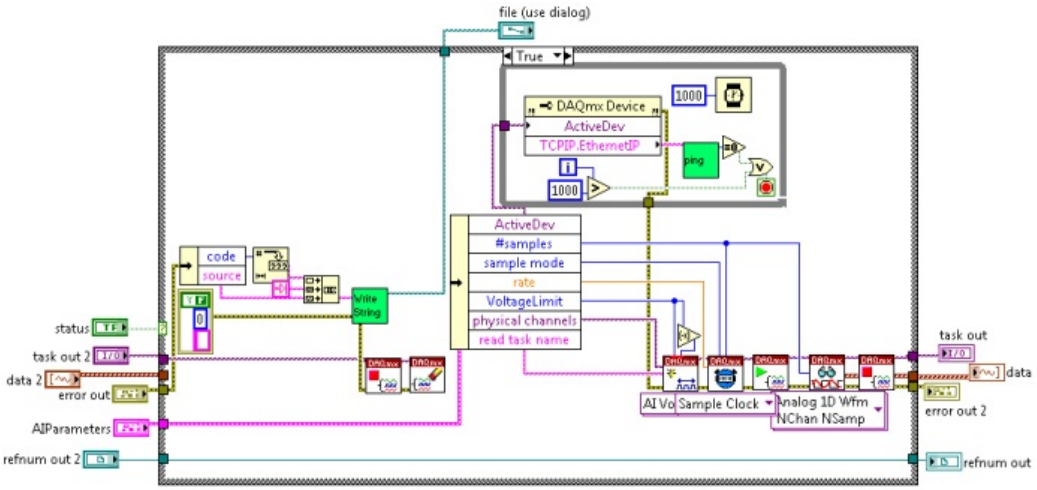

Figure 27: The trouble shooter VI. If an error in the connection between computer and the input card occurred it tries to re-establish a connection and opens up a new task.

Trouble Shooter Should there be no error, the trouble shooter VI will not do anything except that it logs that no error occurred. If an error occurred (for example, the connection to the card was lost) the trouble shooter logs it and then closes the task running at the moment, Figure 27. After that, another while loop is opened up. It tries to get a ping answer from the card chassis using its TCPIP Ethernet IP address (this can be obtained via the router). Should it not be able to get a connection to the chassis, the program will stop. But if there is again a connection, the while loop is closed and a new task is initialized, again with the same procedure as before. After the initialization a readout is performed, and the obtained data is passed on.

The Data is used to obtain the time information in order to log sensor signals and output voltages in a .txt file. The data is also fed into a sub VI that transforms the waveform format to an array of doubles. This array of doubles is then logged, and used to make a waveform chart. Also, it is fed into the off-setter sub VI that subtracts an offset (if set in the user interface) from the signal. The resulting voltage is then used to make the feedback.

The Feedback Sub VI has three inputs, Figure 28a. First, it uses the output voltage of the last iteration. In the first iteration, this is just zero in all channels. Then, it adds half the sensor voltage (already including the offset) onto this value provided that these are not smaller than a threshold

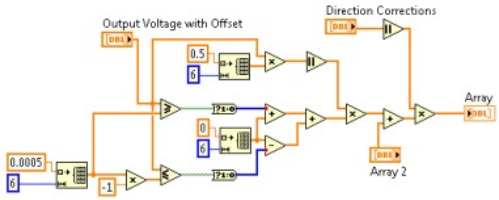

(a) The Feedback sub VI. It takes the output voltage of the former iteration and adds half the sensor signal on it, provided the sensor signal is bigger than a threshold value.

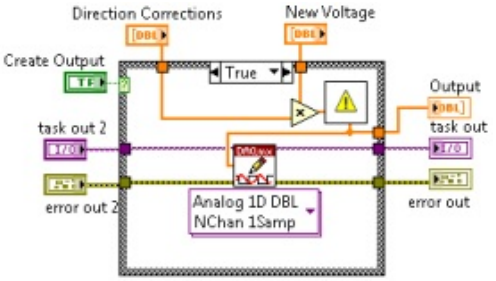

(b) The Output sub VI. It creates an output and ensures that no output is larger than 5 V.

Figure 28: Two of the sub VIs used in the LabView program.

value. In the end, the VI multiplies the output voltage with the "Direction Corrections" array, such that during the running program a coil can be turned off or on. The output of this VI is an array of output voltages.

The Output Creator Sub VI also has three inputs, Figure 28b. The first is a boolean that determines whether or not an output voltage should be generated. The second input are the voltages that should be generated. These are multiplied with the direction corrections. The sub VI with the warning sign then checks that all these voltages are below 5 V and puts them to zero if they are above. Then, the output is created on the output card. The array named "Output" contains the voltages that are effectively applied.

The effectively applied voltages are then displayed in the user interface and also logged in the .txt file. After this, the iteration of the while loop is completed and the program waits one second until it executes it again.

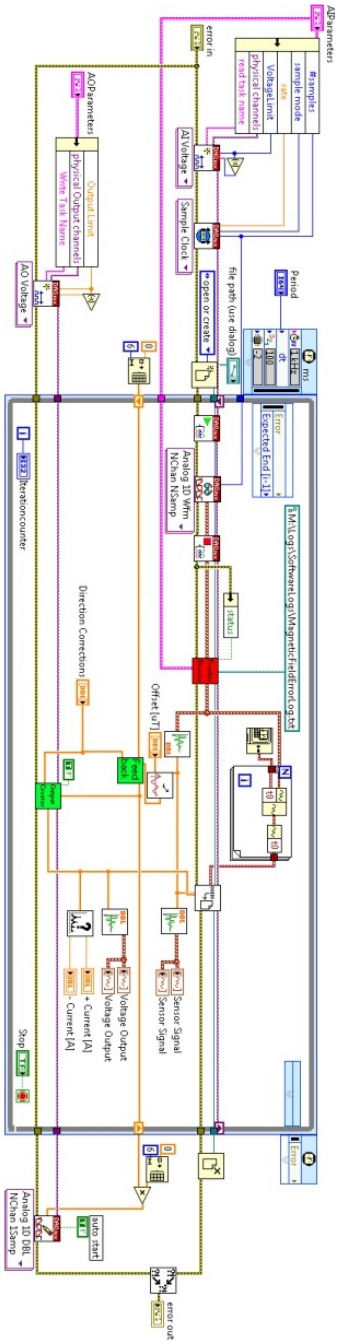

Figure 29: The whole LabView program. The initialization of the tasks and definition of the sample clock is done in front of the while loop which is executed once every second. Then a readout is performed and the sensor data is then used to create an output voltage. The wave chart diagrams in Figure 12 obtain the data from the indicators "Sensor Signal" and "Voltage Output".

ETH

Eidgenössische Technische Hochschule Zürich
Swiss Federal Institute of Technology Zurich

Declaration of Originality

This sheet must be signed and enclosed with every piece of written work submitted at ETH.

I hereby declare that the written work I have submitted entitled

Active Magnetic Field Compensation

is original work which I alone have authored and which is written in my own words.*

Author(s)

Last name	First name
Luethi	Florian

Supervising lecturer

Last name	First name
Wallraff	Andreas

With the signature I declare that I have been informed regarding normal academic citation rules and that I have read and understood the information on 'Citation etiquette' (http://www.ethz.ch/students/exams/plagiarism_s_en.pdf). The citation conventions usual to the discipline in question here have been respected.

The above written work may be tested electronically for plagiarism.

Zuerich, 18.03.2014
Place and date

Florian Luethi
Signature

*Co-authored work: The signatures of all authors are required. Each signature attests to the originality of the entire piece of written work in its final form.

Print form